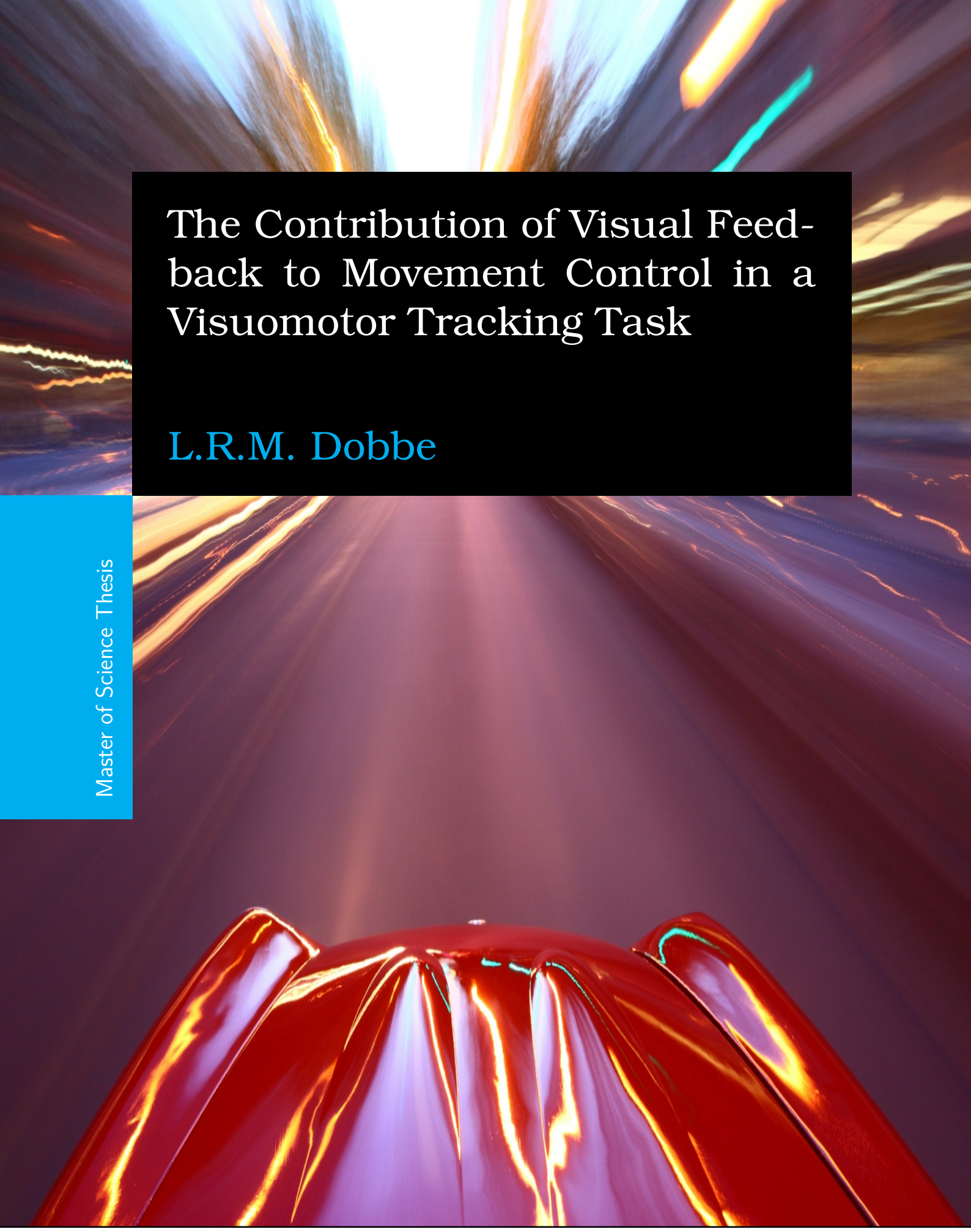

The Contribution of Visual Feedback to Movement Control in a Visuomotor Tracking Task

L.R.M. Dobbe

Master of Science Thesis

TU Delft Delft University of Technology

BioMechanical Engineering Department

The Contribution of Visual Feedback to Movement Control in a Visuomotor Tracking Task

Master of Science Thesis

For the degree of Master of Science in Mechanical Engineering at Delft University of Technology

L.R.M. Dobbe

November 21, 2014

Faculty of Mechanical, Maritime and Materials Engineering (3mE) · Delft University of Technology

motek medical
improving human performance

The work in this thesis was supported by Motek Medical BV. Their cooperation is hereby gratefully acknowledged.

Abstract

The aim of this study was to determine if and how specific characteristics of visual information influence the motor control strategy adopted during a visuomotor tracking task. To this end, twenty healthy subjects and two stroke patients were measured. Changes in wrist joint admittance (i.e., wrist rotations due to external forces) due to specific manipulations of the visual scenery related to task demands (i.e., tolerance, velocity, preview; experiment 1) and related to presentation of visual information (i.e., gain, optical flow density; experiment 2) were quantified using System Identification and Parameter Estimation (SIPE) techniques in order to distinguish between continuous feedback, intermittent feedback and anticipatory feedback control strategies. To this end, a linear physiological model comprising short-latency muscle spindle feedback ánd long-latency visual position feedback was fitted to the experimental data. To study control adaptability, the potential of a linear time invariant (LTI) technique to analyze time variant (TV) control behavior was explored. In both experiments, manipulations of the visual information elicited significant changes in intrinsic and reflexive neuromuscular properties and use of visual feedback. The findings suggest that humans flexibly adapt their use of visual feedback between continuous feedback and intermittent feedback control, dependent of demands on task precision and movement velocity. Anticipatory feedback control was dependent on the amount of future task information available, but was suppressed by high task demands and increased when movements were visually amplified. LTI models can successfully be deployed for the analysis of TV control behavior in tracking tasks, provided that actual movement amplitudes are small. It is concluded that the discussed methods yield potential in the identification of motor control adaptability for the use in diagnostics of movement disorders.

Table of Contents

Acknowledgements **ix**

1 Introduction **1**

2 Materials and Methods **5**
2-1 Experiment . . . 5
2-1-1 Test Subjects . . . 5
2-1-2 Experimental Setup . . . 6
2-1-3 Protocol . . . 8
2-2 Data Analysis . . . 12
2-2-1 Approach . . . 12
2-2-2 Data Pre-processing . . . 12
2-2-3 Task Performance and Control Effort . . . 12
2-2-4 Corrective Steering Power Spectral Density . . . 12
2-2-5 Admittance Analysis . . . 13
2-2-6 Parametric Analysis . . . 13
2-2-7 Time Variant Approach . . . 15
2-3 Statistical Methods . . . 17

3 Results **19**
3-1 Experiment 1 . . . 20
3-1-1 Time Domain Analysis . . . 20
3-1-2 Frequency Domain Analysis . . . 21
3-1-3 Parameter Estimation . . . 23
3-1-4 Time Variant Results . . . 26
3-2 Experiment 2 . . . 29
3-2-1 Time Domain Analysis . . . 29
3-2-2 Frequency Domain Analysis . . . 30
3-2-3 Parameter Estimation . . . 30
3-3 Feasibility Study . . . 32

4 Discussion **33**

5 Conclusions **39**

A Information and Forms **41**
A-1 Information letter to subjects 41
A-2 Informed Consent 44
A-3 Experiment Questionnaire 45
A-3-1 Experiment 1 45
A-3-2 Experiment 2 47
A-4 Pain Questionnaire 49

B Literature Study **51**
B-1 Literature Study: Visual Information in Motor Control 51
B-1-1 Visual Feedback to Motor Command 51
B-1-2 Visual Attributes 52

C Methods **55**
C-1 Hardware Delay 55
C-2 Condition Tables 57
C-3 Perturbation Signal Time Length 58
C-4 Closed Loop Estimator 60
C-5 ARMAX Model Order 61
C-6 Parameter Model Choice 63
C-7 Parameter Model 65

Bibliography **67**

List of Figures

1-1 Key elements involved in movement and interaction with our environment 2

2-1 An overview of the experimental setup 6
2-2 The perturbation signal and its auto spectral density 7
2-3 The virtual environment 8
2-4 Test subject preparation 9
2-5 The conditions for movement tolerance and preview 10
2-6 The conditions for visual gain and optical flow 11
2-7 The parametric model for H 14
2-8 The TV analysis 16

3-1 Time domain analysis results 21
3-2 Intermittency of experiment 1 22
3-3 The admittance plot and a position simulation plot 23
3-4 Low frequent admittances and VAFs for experiment 1 24
3-5 Results neuromuscular parameter estimations 25
3-6 Time variant results 27
3-7 Road influence on TV analysis 28
3-8 Performance and RMSe results for experiment 2 29
3-9 Observed steering delays due to changes in visual gain and optical flow 30
3-10 Results of steering PSD, EMG, admittance and k in experiment 2 31
3-11 Results for patient 2 32

A-1 Questionnaire results of experiment 1 46
A-2 Questionnaire results of experiment 2 48
A-3 Pain questionnaire results 49

C-1 The calculation of the time delay between motor input and visual output 56
C-2 The perturbation signal time length analysis for 8s, 4s, and 2s. 59
C-3 The control scheme for non-parametric analysis 60
C-4 ARMAX model order analysis 62
C-5 The three neuromuscular models 63
C-6 Model choice error boxplots 64
C-7 The parametric model for H 65

List of Tables

3-1 Time variant results 26

4-1 Results summary 36

C-1 The condition table for experiment 1 sorted by visual attribute 57
C-2 The condition table for experiment 2 sorted by visual attribute 57
C-3 Parameter optimization settings 66

Acknowledgements

In the past year, I have had the privilege to perform my graduation project under the supervision of a multi-disciplinary group of people. Firstly, as a biologist and as an engineer, Jurriaan de Groot participated in the weekly meetings and guided the experimental phase of the study. His friendly, accessible attitude and unlimited interest in the human body has led to valuable discussions concerning my work, for which I would like to thank him. Secondly, my gratitude goes out to my personal supervisor from the TUDelft, Erwin de Vlugt. From the moment that I started following courses in neuromuscular control until the end of this graduation project, he has managed to inspire me with is unstoppable optimism, and enthusiasm about motor control of the human body. Furthermore, I thank him for helping me find an internship in Cleveland and for guiding me through the world of System Identification and Parameter Estimation. Finally, as my supervisor from the LUMC, Linda Bank has guided me through the entire course of this graduation project. Apart from a decent theoretical approach to scientific research, she has taught me a great deal of practical concerns in human experiments as well. Her 'no-nonsense', hard working attitude has had a great inspiring effect on me. From the start of the project until the last bit, she has helped me with anything that came up, for which I thank her intensely. Furthermore, I would like to thank her for helping improve my English academic writing skills, which is hopefully reflected in this thesis.

I am also very grateful to Lennart Nordin and Goof van de Weg, who proofread parts of this thesis. Furthermore, I would like to thank my brother, Roel Dobbe, for the inspirational discussions about my work and his feedback on my thesis.

Finally, I would like to thank my parents and friends for their support. I especially thank my girlfriend Willemijn for the healthy dose of distraction and fun during the past half year, which undoubtedly has improved the quality of this thesis.

L.R.M. Dobbe
Delft, the Netherlands

November 21, 2014

Chapter 1

Introduction

Movement facilitates people in self-care, work and recreational activities. Prevalent diseases that impair motor function, including neurogenerative diseases (e.g., Parkinson's disease), neurovascular diseases (e.g., stroke) and musculoskeletal pain conditions (e.g., osteoarthritis), have considerable impact on mobility and manual function and may ultimately result in loss of quality of life (King, 1996).

The execution of movements depends heavily on the ability to use sensory feedback. In literature, roughly three sensory feedback control strategies can be distinguished: 1) *continuous feedback control*, in which the motor output is constantly adjusted based on the actual on-line sensory information (Bays and Wolpert, 2007; Wolpert and Ghahramani, 2000), 2) *intermittent feedback control*, in which the motor commands are only intermittently updated on the basis of sensory information (e.g., feedback control is only activated when errors become too large (Loram et al., 2012; Van Der Kooij and De Vlugt, 2007; Miall et al., 1993), and 3) *anticipatory feedback control*, in which sensory feedback from the past is used to anticipate to external disturbances or movement goals in the future (Krishnan et al., 2012; Sainburg et al., 1999). Although the latter is often referred to as feed-forward control in literature, it can also be interpreted as a feedback control component with a phase lead, since the human body is able to use e.g. visual feedback to anticipate to future states, while feed-forward implies that no feedback information is used to execute movements (e.g., in ballistic movements; Seidler et al. (2004)).

The extent to which these control strategies are invoked in a given situation depends on the task demands (e.g., precision, movement velocity), task knowledge (e.g., prior knowledge, predictability), and the quality of control mechanisms, such as the central nervous system (CNS), muscle spindles (MS), Golgi tendon organs (GTO) and intrinsic muscle properties (e.g., stiffness, damping) as well as the availability and reliability of sensory information (Jacobs, 2002). For optimal use of sensory information, this information is integrated in the CNS by weighing the different sensory information based on their uncertainties (Bays and Wolpert, 2007).

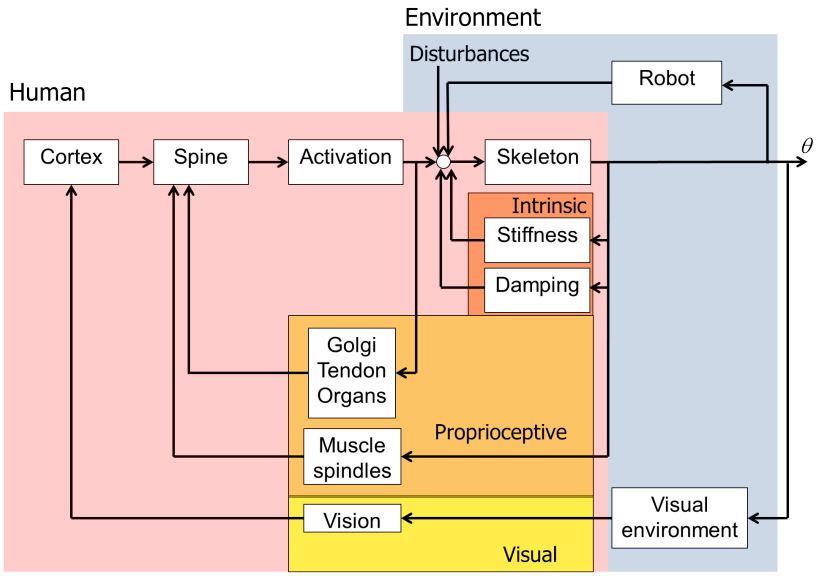

Figure 1-1: Key elements involved in movement and interaction with our environment. Former research mainly focused on the contribution of intrinsic (dark orange) and proprioceptive feedback (light orange) on motor control. The present study also studied the contribution of visual feedback (yellow) to the control of a continuous tracking task. The human interacts with the environment by means of a robot, while being subjected to external disturbances. Movements (θ) are fed back visually via the supraspinal pathways through the cortex and the spine, and through proprioceptive feedback from muscle spindles and Golgi tendon organs to the spine.

Prevalent diseases that affect components of the closed loop chain of motor control influence the quality and the processing of sensory information, which could result in motor dysfunction. Current diagnostic assessment methods mainly focus on the movement performance of a patient with a movement disorder. However, different diseases, affecting different (sub)systems in the closed loop motor chain (i.e. control mechanisms), may result in a similar movement performance, which impedes the identification of the disease and therefore postpones treatment initiation. Hence, to identify the contributing factors of a movement disorder, it is necessary to thoroughly assess the human body mechanically and neurally. Existing techniques are of low resolution or lack the possibility to identify the contributing factors of a movement disorder. Therefore, the clinical community is in need of new clinical tests that invoke and identify contributing (or affected) control mechanisms.

The use of haptic devices in combination with system identification and parameter estimation (SIPE) techniques have shown promising results in the field of the identification of neuromuscular properties (i.e. MS feedback, GTO feedback and intrinsic muscle stiffness and damping), by perturbing a certain joint and analyzing its admittance (i.e., the joint rotation as a result of a force disturbance). Studies have shown significant changes in neuromuscular properties due to the influence of task type (Mugge et al., 2010), changes in mechanical environments (de Vlugt et al., 2002) and disturbance type (van der Helm et al., 2002) in continuous tasks, and in discrete tasks, such as reaching or pointing (Selen et al., 2006a). Moreover, the techniques have been employed to demonstrate the lack of reflex gain adaptation in stroke patients (Meskers et al., 2009). However, there are three limitations which the previously mentioned studies all have in common. Firstly, the studies focused on trials of steady state behavior,

in which it is assumed that subjects behave constantly during the assessment period. The disadvantage of this method is that natural control behavior may be suppressed and that dynamical adaptations of neuromuscular properties cannot be identified. Secondly, coordinated movements, such as playing tennis or steering, are also governed by *visual feedback*, which is not considered in the mentioned studies (see Figure 1-1). A significant amount of studies however, have demonstrated the importance of visual feedback on task performance in both continuous motor control tasks such as position control (Selen et al., 2006a; Hong and Newell, 2008) and force control (Beuter et al., 1995), and discrete motor control tasks such as pointing (Selen et al., 2006b) or tasks involving anticipation to force perturbations (Krishnan et al., 2012). Thirdly, often poor task visualization was provided to subjects. Influence from visual task representation was therefore not considered in the interpretation of the results, while it has the potential to be of importance (Dobbe, 2014).

Therefore, the objective of the present study was to design a protocol in which the neuromuscular system can be assessed by manipulation of visual feedback and quantified by means of SIPE techniques, in a continuous visuomotor tracking task. In specific, the present study aimed to discriminate between continuous feedback control, intermittent feedback control and anticipatory feedback control. Furthermore, the study explored the potential of linear time invariant (LTI) modeling techniques to the analysis of time variant behavior. The protocol was administered to twenty healthy subjects and to two stroke patients in order to examine its feasibility for the possible use in diagnostics.

The protocol aimed to answer the following research questions:

Primary research questions:

1.1 How do changes in task demands (movement tolerance, velocity and preview) and visual information (visual gain and optical flow) affect tracking performance?

1.2 What are the underlying neuromuscular mechanisms (i.e., the control mechanisms) contributing to task performance, i.e., which control strategy is adopted, for the different conditions applied under (1.1)?

1.3 Can LTI methods be deployed to study time variant control behavior?

Secondary research question:

2 Is it feasible to use the protocol and the system identification techniques to assess the neuromuscular system of stroke patients?

For healthy subjects it is hypothesized that primarily anticipatory feedback control will be elicited by high preview (i.e., predictable trajectory), high movement tolerance (i.e., low demands on task precision) and low movement velocity (i.e., low movement frequency). It is expected that the admittance will be relatively high, co-contraction low and that neuromuscular contributions (i.e., MS feedback) will be low. In contrary, primarily continuous feedback control may be adopted in case of low preview (i.e., unpredictable trajectory), low tolerance and high movement velocity (i.e., high demands on task precision) (Selen et al., 2006a). It is expected that the admittance will be relatively low, co-contraction high and that neuromuscular contributions will be high (excitatory, as described in position tasks in Mugge et al.

(2010)). Moreover, it is anticipated that visual feedback will be used (more efficiently) if tracking errors can easily be perceived (i.e., if visual feedback is presented with appropriate gain, density and intensity). Presumably, stroke patients are not (or to a lesser extent) able to adapt their control strategy to changing conditions, with heavier reliance on visual feedback for controlling their movements, which may provide useful insights into the integrity and adaptability of the system involved in motor function in these patients.

Chapter 2

Materials and Methods

2-1 Experiment

The present study assessed the effects of visual attributes on motor control in two separate experiments. Experiment 1 assessed the effects on task demand by varying the movement tolerance, velocity and preview and experiment 2 assessed the influence of visual information per se, i.e., without changing task demands, by varying visual gain and optical flow.

2-1-1 Test Subjects

Twenty healthy adults (6 male, 14 female; age 50 - 76) with normal function of both arms and normal or corrected to normal eye vision participated in the experiment. Minimum age was restricted to 50 years, in order to match the expected age of stroke patients. Two stroke patients were recruited from regular clinical care to examine feasibility of the assessment. Each subject was contacted by phone and subsequently informed and invited by written letter or e-mail (see Appendix A-1). All subjects gave informed consent and the ethics committee of the Leiden University Medical Center approved the study.

Sample Size Calculation

Sample size calculations were based on data from a previous (unpublished) study on wrist joint admittance in 33 healthy participants under two conditions: a relax task (i.e., 'do nothing') and a position task (i.e., 'resist movements'). Using a method very similar to the one that was used in the present study, this study showed an average admittance of 0.71 $\pm$ 0.30 rad/Nm during the relax task and 0.12 $\pm$ 0.07 rad/Nm during the position task. These tasks were expected to reflect the extremes of the present study. The calculations were based on the premise that a difference in admittance of 0.20 rad/Nm between two conditions was detected, which yielded a sample size of 20 subjects (difference = 0.20; SD = 0.30; power 0.8; $\alpha = 0.05$; twosided; paired t-test; (Snedecor and Cochran, 1980)).

2-1-2 Experimental Setup

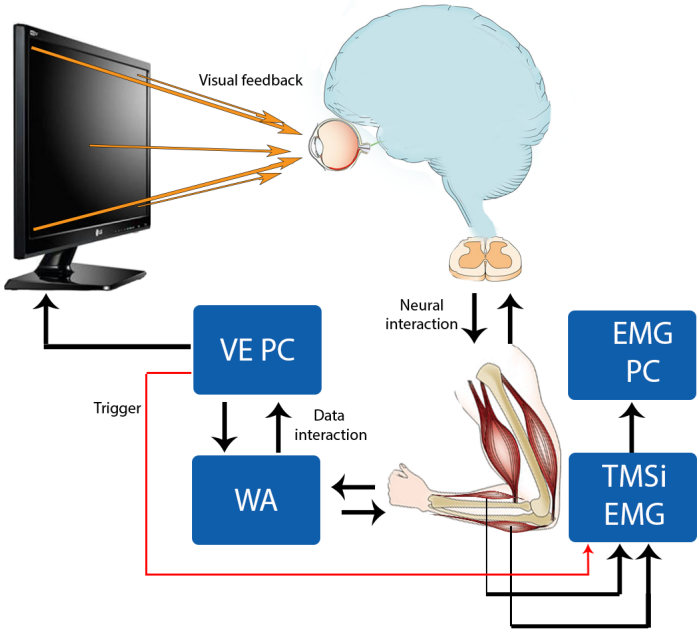

Figure 2-1: An overview of the experimental setup. Subjects interacted with the Wristalyzer (WA). Data was collected and generated by the virtual environment PC (VE PC) and EMG data was measured by electrodes and captured by a TMSi EMG device and subsequently stored in the EMG PC. Data recording was synchronized by means of a trigger, controlled by the VE PC.

Subjects controlled the lateral movements of a virtual car by wrist flexion and extension movements, while they needed to keep the car between the boundaries of a curvy road. The position of the car and the road, as well as the rest of the virtual environment (VE) (see Section 2-1-2) were displayed on a TV monitor.
Figure 2-1 presents an overview of the experimental setup. Angular position of the handgrip and the torque acting on the handgrip were measured by the Wristalyzer (WA; MOOG FCS). The subjects' right forearm was placed in the apparatus with the thumb up and the palm facing inwards and fixated by two foam padded straps at the proximal and distal side of the forearm. The elbow was supported to prevent rotations of the forearm and the wrist axis of rotation was aligned with the hand grip axis of rotation. The elbow was supported by a holder that prevented rotations of the forearm. The device measured the rotation and the torque acting on the hand grip. Control strategy was derived from wrist admittance by means of SIPE techniques. Therefore, small unpredictable pseudo-random force perturbations (1.25 - 20 Hz) were applied to the wrist (see Section 2-1-2).
Virtual environment generation, as well as measurement data collection and synchronization was done by a software package D-Flow (MOTEK Medical, Amsterdam, The Netherlands). The total time delay, from mechanical input (WA movement) to visual output (on the TV monitor), was approximately 135 ms (see Appendix C-1). The virtual environment was developed by means of block oriented programming and by programming in the Lua 5.0 programming language (Ierusalimschy et al., 1998), which was embedded in D-Flow.
A 100 Hz 60" flat screen TV monitor was used to present the visual environment.
Electromyography (EMG) recordings of the wrist flexor muscle (flexor carpi radialis; FCR)

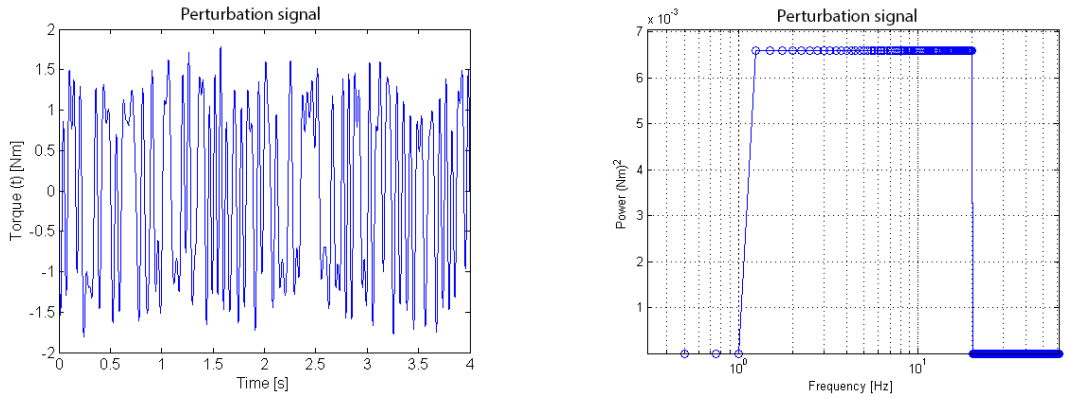

(a) **(b)**

Figure 2-2: The perturbation signal (a) and its auto spectral density (b). The 4-s perturbation signal consisted of a full power spectrum over $f = 1.25 - 20$ Hz with $\delta f = \frac{1}{T} = 0.25$ Hz.

and the right arm wrist extensor muscle (extensor carpi radialis; ECR) were measured unfiltered at 2000 Hz and synchronized by means of a trigger by a TMSi EMG recording device (see Figure 2-1).

Perturbation Signal Continuous pseudo-random multi-sine force perturbations on a frequency bandwidth of 1.25 to 20 Hz ($\delta f = 0.25Hz$; see Figure 2-2) were exerted to the wrist for the use of SIPE techniques. The perturbation signal was designed in the frequency domain with a constant power value and a randomized phase value, uniformly distributed between 0 rad and 2π rad, and transformed to the time domain by inverse Fourier transformation. The full perturbation spectrum was implemented in a 4-s time window (i.e., the length of the perturbation signal) to be able to study control changes in a relatively short period.

Virtual Environment The environment consisted of constant environmental aspects, such as grass, trees and wind mills, a road (consisting of two sinusoids) which defined the curved tracking path (see Figure 2-3b) and a car (which was controlled by the test subject through the WA) (see Figure 2-3a).

The D-Flow unit (DFU) is introduced to understand the dimensions of the VE. The VE consisted of a blocked grid space, in which every block is expressed by 1 by 1 by 1 DFUs. The camera surface (i.e., the 2D grid size projected on the TV monitor (the "look through window")) was 4 DFUs in width and 3 DFUs in height. Therefore, the physical quantity of 1 DFU can be translated to 1/4 of the TV monitor's width, which is approximately 0.35 m. The camera's vertical field of view (FoV) was 75 ° (Figure 2-3). The configuration of the virtual environment and the visual attributes that defined the conditions were also expressed in DFUs.

The road curvature consisted of two sinusoids, which were dependent of the velocity and therefore had a frequency range of 0.1 - 0.3 Hz. The low road frequency was expected to prevent interference with the perturbation frequencies (1.25 - 20 Hz), which could result in a low coherence (i.e., a non linear relation between the input perturbation and the output

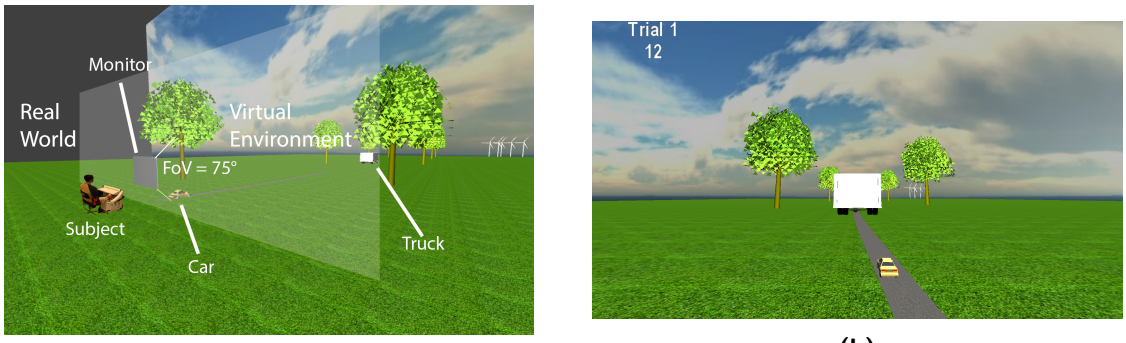

(a) (b)

Figure 2-3: The VE from sideways (a) and from the subject's perspective (b). The VE consisted of a landscape with trees, windmills, a sky and a road. The subjects controlled the car and had to keep the car between the boundaries of the road.

movement). A first order filter ($\tau = 0.1s$) was applied to the car position signal to minimize the effect of the high frequent force perturbation.

Questionnaires A custom made questionnaire was used to assess the subject's experiences regarding various aspects of the experiments (see Appendix A-3). Handedness was assessed using the Edinburgh Handedness Inventory (Oldfield, 1971). After the experiment, a questionnaire was used to assess pain before, during and after the experiment (on a scale from 0-10, with 0 = no pain and 10 = unbearable pain; see Appendix A-4) to assess the physical and mental impact on healthy subjects and patients. This was used as a criterion for the feasibility of the protocol.

2-1-3 Protocol

Preparation

All subjects were assessed in the Laboratory of Kinematics and Neuromechanics of the Department of Rehabilitation at the LUMC. After a short briefing of the study procedure and signing the informed consent (Appendix A-2), hand dominance was assessed. Surface electrodes were used to obtain EMG from the FCR muscle and the ECR muscle of the tested arm, after cleansing of the skin. The right arm (or, in stroke patients, the most affected arm) was attached to the WA (Figure 2-4b). Subjects were seated in a chair 1.5 m in front of the TV monitor in normal upright sitting posture with their feet supported. For the purpose of normalizing EMG recordings, subjects performed two isometric Maximum Voluntary Contractions (MVC) in each direction (i.e., twice in extension and twice flexion direction).

Prior to the start of the experiment 1, subjects performed a practice trial, which consisted of the proposed easiest and hardest conditions of the experiment. During this practice trial, the appropriate perturbation power was selected, i.e., the perturbation power that resulted in linear movement behavior (i.e., wrist rotations within approximately 1° around the center of the wrist) and high coherence (> 0.7 for all frequencies) to meet the error criteria of the LTI model used for data analysis (see Section 2-2).

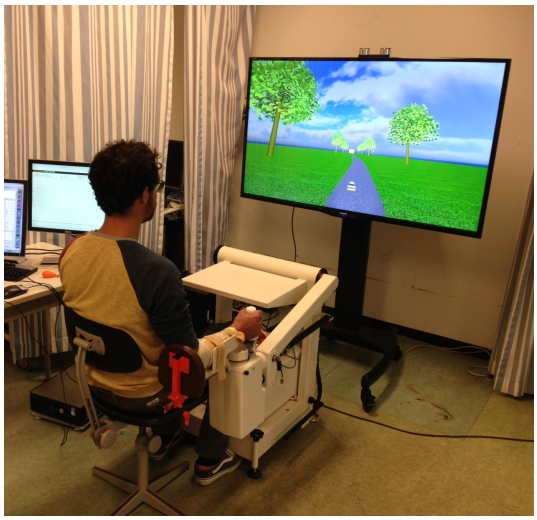

(a)

(b)

Figure 2-4: The setup with test subject (a) and the fixation of the arm to the WA (b). Subjects were seated approximately 1.5 m in front of the TV monitor, and fixated to the WA, by means of two foam padded straps around the arm and a pressure pad at the elbow, in upright position with their feet supported.

Task instruction Subjects performed a sub-maximal visuomotor tracking task, in which the objective was to maintain the car within the boundaries of the road. The task instruction to the subjects was as follows:

"You control the car position from left to right. You need to keep the car on the road at all times, while you are being subjected to small force perturbations. You may use the full width of the road. As long as the car is on the road you are doing fine."

At the start and the end of the experiment, and during transitions between conditions, the visual attributes of the virtual environment changed fluently (i.e., linearly) from one to another in 10 seconds, which provided the subject sufficient time to adapt to the new condition.

Experiment 1: Effect of Task Demands

In experiment 1, it was examined if and how task performance and the underlying neuromuscular properties of the wrist were influenced by specific changes in task demands, which were induced by systematic manipulation of three visual attributes: 1) *movement tolerance*, which was defined by the road width (low (0.25 DFU), medium (0.5 DFU) and high (1 DFU), see Figure 2-5), 2) *velocity* (low (4 DFUs/s and road frequency $f_{road} = 0.08$ Hz), medium (8 DFUs/s and $f_{road} = 0.16$ Hz) and high (12 DFUs/s and $f_{road} = 0.24$ Hz)) and 3) *preview*, which was defined by a view obstruction due to a truck (low (2 DFUs), medium (10 DFUs) and high (50 DFUs), see Figure 2-5).
To study control adaptability to changes in the visual environment, the hardest (i.e., low movement tolerance, high velocity and low preview; denoted as 'hard curvy' (HC)) and easiest (i.e., high movement tolerance, low velocity and high preview; denoted as 'easy curvy'

(EC)) conditions were deliberately placed behind each other in the condition order twice: from hard to easy and from easy to hard. Two equivalent conditions with a *straight road* ('hard straight' (HS) and 'easy straight' (ES)) were added to study the influence of the curvy road to the outcome parameters (see Section 2-2-7). All conditions were assessed only once, except for HC and EC (twice). This resulted in a total of 31 conditions, which were presented in random order. Each condition was 30-s long, followed by a 10-s transition in which the conditions from the previous condition changed linearly to the next condition. The conditions were presented in blocks of three, which were followed by a 40-s pause, in which the performance of the previous block was fed back to motivate the subject.

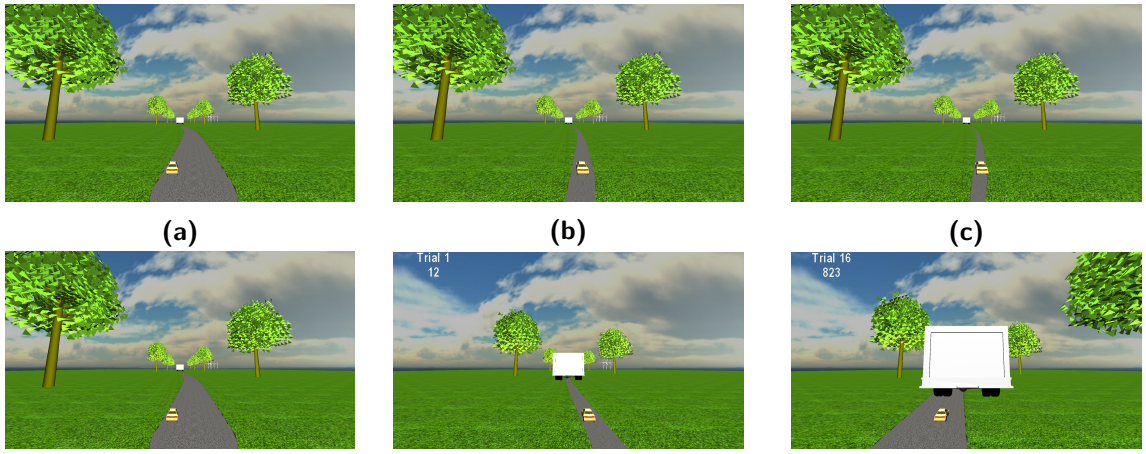

Figure 2-5: The conditions for high (a), medium (b) and low (c) movement tolerance and for high (d), medium (e) and low (f) preview. The road width determined the degree to which subjects' movements were tolerated. The truck obstructed sight for low preview and medium preview. For high preview, the truck drove towards the horizon.

The total measurement time for experiment 1 was 26 minutes and 53 seconds. Extra pause time was allowed if the subject needed more time to recover. Furthermore, in case the subject was distracted during a measurement, the condition in question was repeated at the end of the experiment.

Experiment 2: Effects of Visual Information

In experiment 2, it was examined if and how task performance and the underlying neuromuscular properties of the wrist were influenced by specific changes in visual information without affecting task demand, which were induced by systematic manipulation of two visual properties (visual gain and optical flow). The *visual gain* was defined as the degree to which objects and their movements are visually amplified (see Figure 2-6). Changes in the road width, the car size and the movement gain of the car position (which were equally scaled) created a zoom effect (e.g., if the car size was doubled, the road width and movement gain were also doubled). The visual gain was defined by three settings: Low (0.5), medium (1, as in experiment 1) and high (2). The *optical flow* was represented by the presence or absence of a tunnel (see 2-6c). The combination of the two visual attributes resulted in a total of 6 conditions.

(a) **(b)** **(c)**

Figure 2-6: The conditions for high (a), medium (b) and low (c) visual gain and an example for the tunnel (c). Task demands remained the same for all conditions (i.e., the gain between the WA and the position on the screen were equally scaled with the car size and road width).

The virtual environment and the process of experiment 2 were equal to those of experiment 1. The total measurement time for experiment 2 was 4 minutes and 40 seconds.

2-2 Data Analysis

Matlab (The Mathworks Inc., Natick MA, version R2014a) was used to process all the data analyses.

2-2-1 Approach

The data were analyzed in the time domain by signal analysis and in the frequency domain by means of SIPE techniques and power spectral densities (PSD).

2-2-2 Data Pre-processing

The measured rotation and torque data were first up-sampled to the WA sampling frequency of 2048 Hz, for synchronization with the perturbation signal (using the trigger data). Subsequently, the measured signals were filtered with a third order Butterworth bandpass filter (2 Hz $\leq f \leq$ 20 Hz) and down-sampled to a frequency of $f_s = 128$ Hz to reduce computational cost.
EMG data were filtered with a third order Butterworth band pass filter ($\omega_{cut-high} = 10Hz$, $\omega_{cut-low} = 0.1Hz$) to remove high frequent responses and low frequent interference (e.g., due to movement of wires) and subsequently corrected for offsets by subtracting the average recorded EMG value. EMG recordings of each muscle were normalized to the subject's corresponding MVC value and presented as percentage of the MVC.

2-2-3 Task Performance and Control Effort

Task performance was assessed to study the effects of task demands on task execution. It was described by the percentage of time that subjects could keep the car between the boundaries of the road. Most test subjects tried to keep the car at the center of the road at all times (see Appendix A-3). Therefore, the control effort was defined as the root mean squared error (RMSe) of the car position with respect to the road center position. Delayed steering (positive delay) and anticipatory steering (negative delay) were identified by minimizing the difference between the car position and the road center, with time as the optimization variable. EMG recordings were evaluated to determine control effort in terms of co-contraction.

2-2-4 Corrective Steering Power Spectral Density

Power spectral densities (PSD) of unfiltered position output data were analyzed to investigate the influence of the conditions on the power of steering corrections. In the ideal case, the full steering power would be reflected in the tracking frequencies of the road (i.e., 0.08 - 0.24 Hz). However, due to inaccuracies in motor outputs (e.g., movement under- and overshoots), steering movements have to be corrected by higher frequent corrective movements, which can rise up to 1 Hz (in the case of a visual delay of 200 - 300 ms (Miall and Jackson, 2006), which was the case in this study ($\approx$ 200 ms, consisting of a hardware time delay (see Appendix C-1) and imposed delay by a first order visual filter)). Therefore, the relative power within the 0.3 - 1 Hz bandwidth was calculated as a percentage of the total bandwidth (0.01 - 1 Hz) in which steering actions can be identified.

2-2-5 Admittance Analysis

ARMAX time modeling The low-frequency admittance (i.e., the average of all frequency points below 4.5 Hz) was determined to enable easy interpretation of the condition effects on admittance. The full frequency bandwidth admittance was used for the parameter model fit (see Section 2-2-6). The coprime factorization method in combination with a closed loop estimation technique (Appendix C-4) was used to identify the contribution of the human to the admittance, which was estimated by means of the frequency response function (FRF) of an AutoRegressiveâĂŞMoving-Average model with eXogenous inputs (ARMAX model; $n_a = n_b = n_c = 8, n_k = 0$, see Appendix C-5). For every recorded condition (30 s), 5 seconds were subtracted from the start and the end to discard motor adaptations, which resulted in analysis windows of 20 seconds. The FRF was distributed over 100 equally log-spaced frequency points between 2 Hz and 20 Hz, instead of 1.25 Hz to 20 Hz, to minimize influence from corrective steering responses (see Section 2-2-4).

Validation The validity of the data is described by the coherence, which is a normalized measure for the linear relationship between the spectral data of the force perturbation ($T_D(s)$) and the measured position ($Y(s)$) or the measured torque ($T(s)$) (Laplace notation):

$$\hat{\Gamma}^2_{T_D Y}(s) = \frac{|\hat{S}_{T_D Y}(s)|^2}{\hat{S}_{T_D T_D}(s) \cdot \hat{S}_{YY}(s)} \tag{2-1}$$

Where a high coherence (close to 1) denotes a linear relationship between Y and T_D and a low coherence indicates non-linear control behavior and/or influence from noise.

The quality (validity) of the ARMAX model is described by the Variance Accounted For (VAF) and was used to assess the results:

$$VAF_{Y(t) \to Y(t)_{sim}} = \left(1 - \frac{VAR(Y(t) - Y_{sim}(t))}{VAR(Y(t))}\right) \cdot 100 \tag{2-2}$$

Where,

$Y(t)$ = The measured position.
$Y_{sim}(t)$ = The ARMAX model simulated position.

Equation (2-2) describes the variance percentage of $Y(t)$ that can be explained by $Y_{sim}(t)$ of the identified model. 0.25 seconds was removed from the start and the end of the simulations, to exclude transient effects from the simulation to the calculation of the VAF.

2-2-6 Parametric Analysis

The model A parametric model was fitted to the admittance (see Figure 2-7) to obtain neuromuscular parameters. The model was adopted from Schouten et al. (2008) and adapted to meet the physical properties of the wrist joint (see Appendix C-6). Furthermore, an extra

long-latency feedback loop was added to model the influence of visual feedback. The model describes the admittance with 7 free parameters (i.e., parameters which are optimized) and 4 fixed parameters (i.e., parameters with a constant value). The free parameters describe the wrist inertia (I_{wr}), the intrinsic muscle stiffness and damping (k and b), muscle spindle feedback (velocity feedback gain k_v and neural time delay τ_d) and visual feedback (position feedback gain k_{vis} and neural time delay τ_{vis}). The fixed parameters describe the activation dynamics (H_{act}; the relative damping ($\beta = 0.7$) and the activation bandwidth $f_0 = 2.5$ Hz, adopted from Schouten et al. (2008)), the visual filter (first order filter H_{vf} with $\tau_{vf} = 0.1$) and the identified visual delay ($\tau = 0.135s$). The road position (X_{ref}) was only fed back visually.

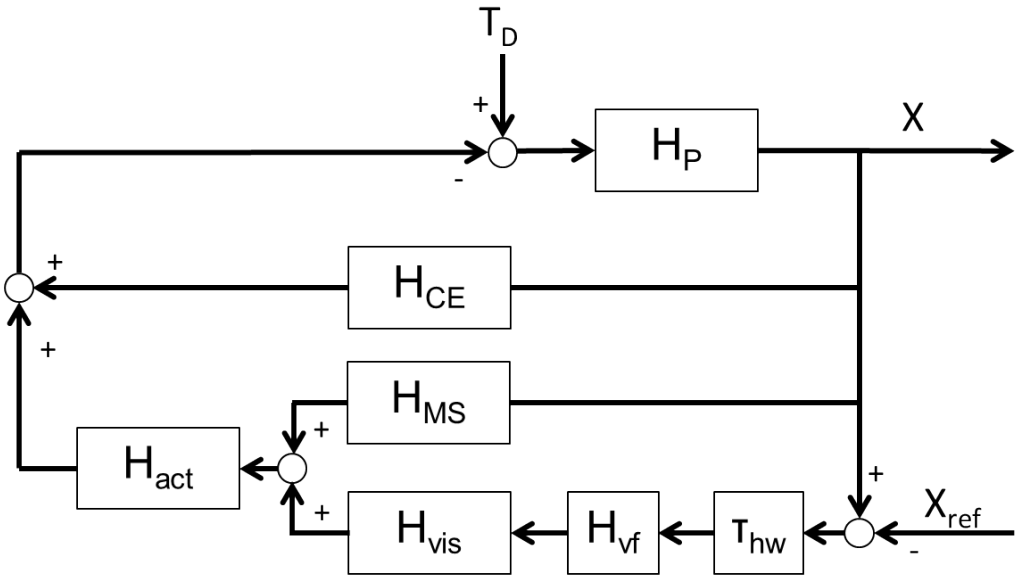

Figure 2-7: The parametric model for H. The human wrist (H_P) is perturbed by the force perturbation signal T_D and perturbed visually by the position reference X_{ref}. The wrist intrinsic properties (H_{CE}), muscle spindle feedback (H_{MS}) and visual feedback (H_{vis}) are used to correct for these disturbances. H_{act} denotes the activation dynamics of (supra)spinal muscle force input signals. Visual feedback was delayed artificially due to hardware delays (τ_{hw}) and filtered visually (H_{vf}). X is the measured output rotation of the wrist.

The dynamic systems in Figure 2-7 denote the following:

$$H_p = \frac{1}{I_{wr}s^2} \tag{2-3}$$

The passive wrist dynamics, described by the wrist inertia.

$$H_{CE} = bs + k \tag{2-4}$$

The contractile elements (active dynamics) of the wrist joint, described by the muscle stiffness k and damping b.

$$H_{MS} = k_v s e^{-\tau_{ms} s} \tag{2-5}$$

Reflexive muscle spindle velocity feedback, described by a velocity gain k_v and a neural time delay τ_d.

$$H_{vis} = k_{vis} e^{-\tau_{vis} s} \tag{2-6}$$

Visual feedback, described by a position gain k_{vis} and a neural time delay τ_{vis}.

The parameter model was fitted by means of a non-linear least squares optimization. The optimization settings (lower- and upper parameter boundaries, optimization properties) can be found in Appendix C-7.

Validation The parameter fit was validated by the error between the FRF of the ARMAX model and the parametric model. The individual contribution of the parameters to the fit was evaluated by the standard error of the mean (SEM). The SEM value indicates the deviation of the parameter value with respect to its optimal value. The lower the SEM value, the higher the contribution of the parameter to the model fit.
The error function was defined by:

$$Res(f) = H_{ARMAX}(f) - H_{par}(f) \tag{2-7}$$

$$E_{fit} = \frac{Res^T(f) \cdot Res(f)}{n_{fit}} \tag{2-8}$$

Where $Res(f)$ is the residual function of the fit, E_{fit} the model fit error and n_{fit} the amount of data points on the f-axis.
The SEM was defined by:

$$SEM = \sqrt{\frac{1}{n_{fit}} I (J^T J) E_{fit}} \tag{2-9}$$

Where I denotes the identity matrix and J the Jacobian matrix of the error with respect to all parameter values.

2-2-7 Time Variant Approach

The LTI (parameter) model, as described in the previous section, was used to execute a linear time variant (LTV) analysis by sliding a short analysis window over the time data in steps of 1 second (see Appendix C-3 for an explanation about the window time length). The time variant (TV) analysis assumes LTI behavior within the window and allows for LTV behavior between the windows. Each analysis determines the admittance by means of an ARMAX model of the specified window and performs a parameter model fit to obtain neuromuscular properties, whereafter the window slides 1 second over the data and repeats itself until the end of the dataset is reached.

Test Case: Transition between conditions As a test case for the method, transitions from HC to EC were analyzed for stiffness k, since control changes were expected to be largest between these conditions. TV results of k were analyzed on control change threshold time (i.e., the time difference between the start of the transition and the moment on which the parameter value changed more than the standard deviation of HC with respect to the mean value) and control change magnitude (i.e., the parameter value difference between the conditions) with a time window of $t_w = 2$, 4 and 8 s, to study the influence of the time window size. Furthermore, the control change slope of the parameters was determined as the tangent of the TV response of the parameters at the control change threshold time (see Figure 2-8).
Parameter responses were normalized to the mean value of HC and low pass filtered to reduce variability ($\omega_{cut} = 0.075$ Hz, order 4, without phase lag)). Results were validated by the VAF (Equation (2-2)) and the SEM value per parameter (Equation (2-9)).

Road and steering influence Road influence on steering was investigated. The TV approach was applied to four conditions: HC, EC and HS, ES, as described in Section 2-1-3. VAFs, SEMs and coherences were compared to investigate the influence of steering on the quality and reliability of the obtained data. Cross correlations between the road track center and the obtained outcome parameters were determined for HC and EC to study road curvature influence on the model parameters. Road center position data was resampled to 1 Hz to comply with the sample rate of the obtained outcome parameters.

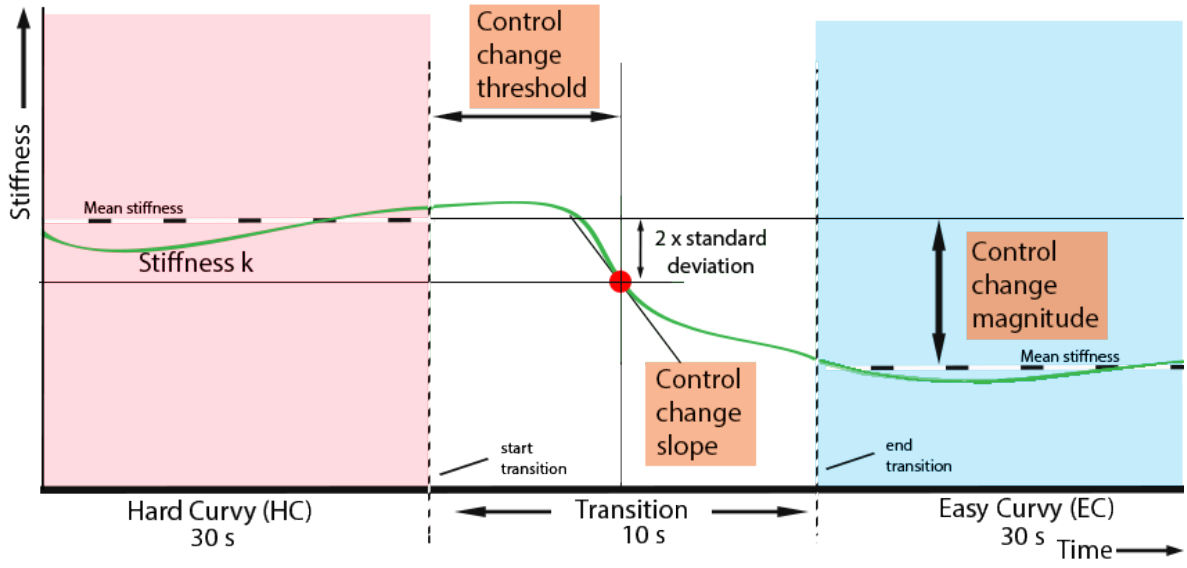

Figure 2-8: The TV analysis. A time window of $t_{window} = 2$, 4 or 8 s slides in steps of 1 second over the data and estimates an ARMAX model for each analysis and fits a parameter model to obtain neuromuscular parameters. As a test case, control changes were quantified by control change threshold (t), control change magnitude and control change slope (orange boxes). The green line describes the possible response of stiffness k over the course of HC to transition to EC. The red dot denotes control change threshold time value of k.

2-3 Statistical Methods

Normality of the distribution of (transformed) continuous variables was tested using the Kolmogorov-Smirnov test and by inspecting PP-plots. Mauchly's test was used to check the assumption of sphericity. For the healthy subjects, measures of task performance, admittance and neuromechanical parameters were compared between conditions using repeated measures ANOVA to evaluate the effects of task demands (preview, movement tolerance, velocity) and visual information (visual gain, optical flow). Simple effects analysis were used to scrutinize significant interaction effects. Post hoc analyses of significant main effects were performed using two-tailed paired t-test with Bonferroni correction. All values are presented as mean +/- standard deviation, unless stated otherwise. Statiscal analysis was performed using SPSS (PASW Statistics 22.0, SPSS Inc., Chicago, Il, USA).

Chapter 3

Results

Data of two subjects were excluded from analysis. The first subject was used as pilot subject and therefore did not experience the exact same conditions as the other subjects. A second subject did not meet the inclusion criteria. Therefore the test population for analyses was $n = 18$.
Results of visual feedback gain, admittance (experiment 1), visual feedback gain and extensor EMG (experiment 2) were log transformed for the sake of a normal distribution for the statistical analyses. Furthermore, no statistical analysis was performed on task performance due to non-uniformal distributions of the results, for both experiment 1 and 2. For clarity, all outcome parameters are presented in their own units.
Due to a programming error in the experiment application, it was impossible to perform the TV analysis to the transition from the easiest to the hardest condition. Therefore, the TV analysis was solely performed on the transition from the hardest to the easiest condition (i.e., from HC to EC).

3-1 Experiment 1

3-1-1 Time Domain Analysis

Performance From Figure 3-1a it appears that both tolerance and velocity have an effect on performance. Performance decreased especially for low tolerance with respect to medium and high tolerance, which was more pronounced in combination with an increase in velocity, especially for low tolerance and to a lesser extent for medium tolerance. The results for preview appeared to be equivalent for each level of preview.

RMS error A main effect was found on RMS error for tolerance ($F(1.30, 22.02) = 227.35$, $p < 0.001$, $\eta_p^2 = .93$), which was complemented by an interaction effect between preview and tolerance ($F(4, 68) = 9.71$, $p < 0.001$, $\eta_p^2 = .36$; see Figure 3-1c) and between tolerance and velocity ($F(4, 68) = 4.25$, $p = 0.004$, $\eta_p^2 = .20$); see Figure 3-1d).
Post-hoc analyses demonstrated a relatively higher control effort (i.e., lower RMS error) for low preview as compared to the medium and high preview conditions (Figure 3-1c) for medium and high tolerance. RMSe especially decreased for decreases in tolerance, regardless of the preview. However, the RMSe drop was more significant for high and medium preview than for low preview.
Figure 3-1d shows clear differences in RMSe between the three velocity levels, where differences are more pronounced for low and medium tolerance, with respect to high tolerance. Furthermore, increases in tolerance resulted in increases in RMSe, especially between medium and high tolerance.

Steering delay and anticipation Main effects were found for preview ($F(2, 34) = 26.61$, $p < 0.001$, $\eta_p^2 = .61$) and tolerance ($F(1.15, 19.59) = 10.02$, $p = 0.004$, $\eta_p^2 = .37$) on steering delay, which were complemented by an interaction effect between tolerance and preview ($F(4, 68) = 20.68$, $p < 0.001$, $\eta_p^2 = .55$).
A post-hoc analysis of the interaction effect showed that a low and medium tolerance and low preview independent of each other resulted in delayed steering (i.e., a positive time delay; see Figure 3-1b). For low preview the steering delay increased for an increase in movement tolerance. In contrary, steering delays decreased for medium and high preview for an increase in tolerance. Anticipatory steering (i.e., a negative time delay) was found for a high movement tolerance and a medium or high preview.

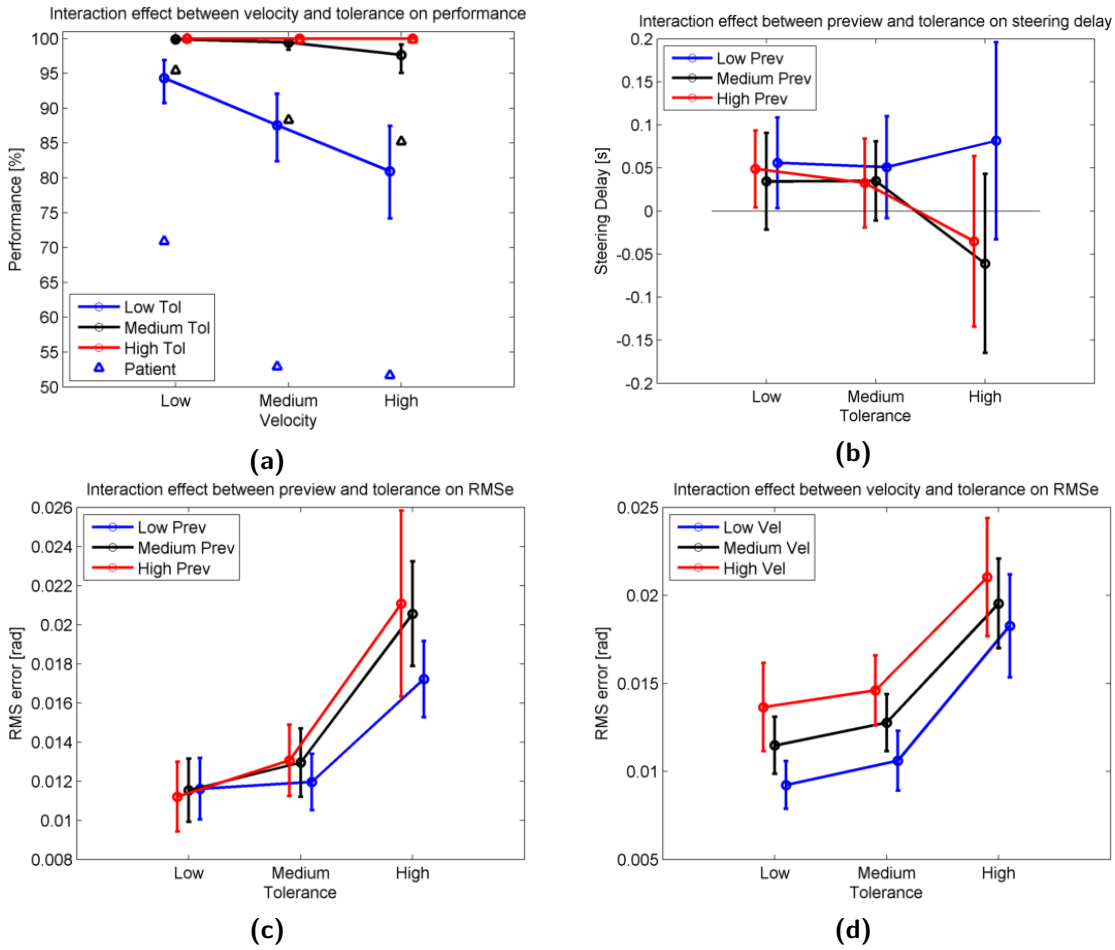

Figure 3-1: (a): The interaction effect between velocity and tolerance on the performance (i.e., the time percentage of the car between the boundaries of the road per condition). (b): The interaction effect between tolerance and preview on the steering delay. The black horizontal line denotes the line that divides delayed steering (positive delay) from anticipatory steering (negative delay). (c) and (d): The interaction effect between preview and tolerance (c) and velocity and tolerance (d) on the RMS error between the car position and the road center position. The abbreviations 'Prev', 'Tol' and 'Vel' stand for 'Preview', 'Tolerance' and 'Velocity', respectively. The plots describe the means (circles) and the SDs (error bars) over n = 18 subjects.

3-1-2 Frequency Domain Analysis

Corrective steering PSD For powers within the 0.3 - 1 Hz frequency band with respect to the 0.03 - 1 Hz frequency band, the observed main effects of preview ($F(2, 38) = 7.62$, $p = 0.002$, $\eta_p^2 = .29$) and velocity ($F(1.52, 28.9) = 163.89$, $p < 0.001$, $\eta_p^2 = .90$), were complemented by a three-way interaction effect between preview, tolerance and velocity ($F(3.52, 66.82) = 2.94$, $p < 0.032$, $\eta_p^2 = .13$). Figure 3-2c illustrates that steering PSD significantly increased due to increases in velocity, where effects were greater in combination with low tolerance and somewhat attenuated in combination with medium preview. Furthermore, as expected, steering PSDs were low for the straight road conditions (Figure 3-2a).

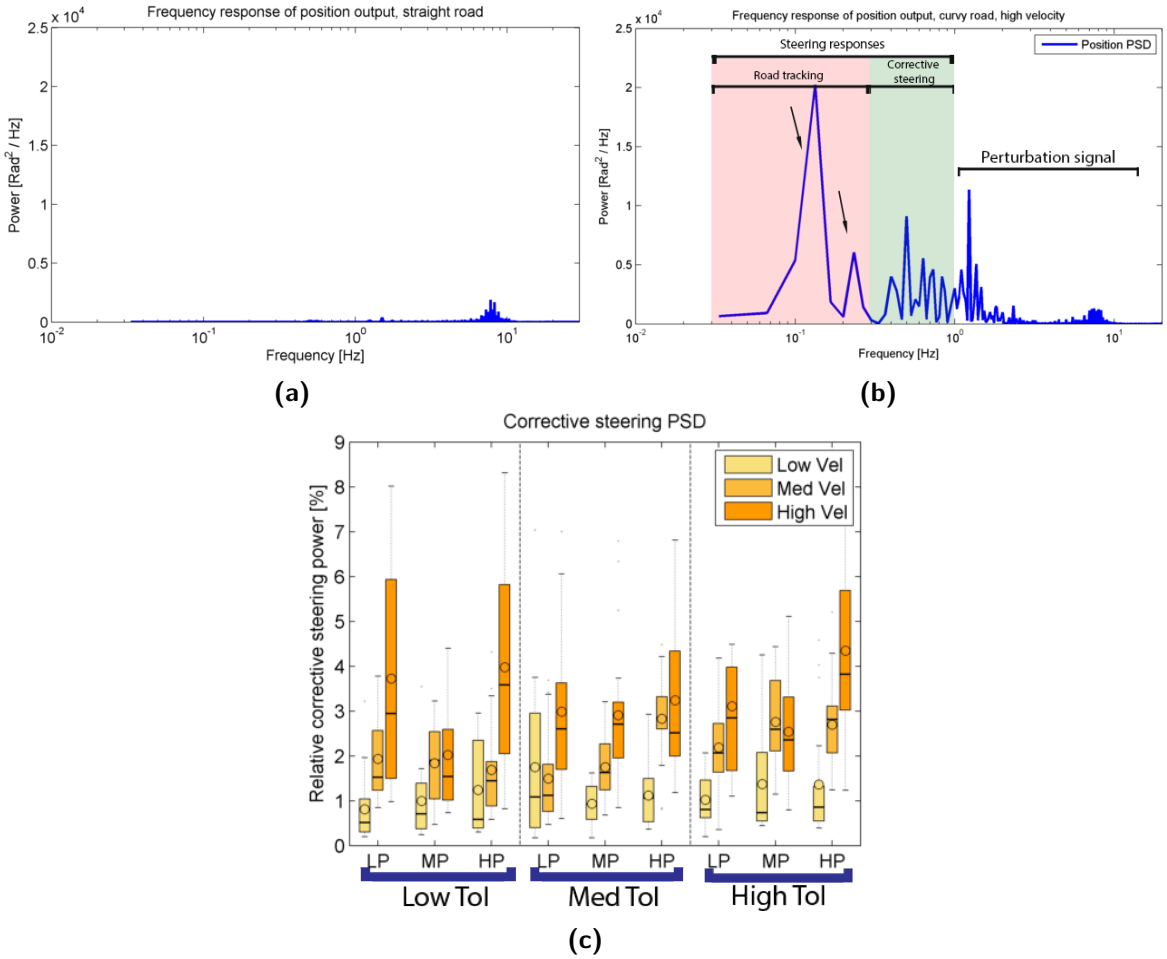

Figure 3-2: (a): PSD of the position output for a typical subject for a straight road condition (ES) (a) and high velocity, curvy road condition (HC) (b) within the 0.03 - 20 Hz bandwidth. Responses originate from road tracking frequencies (0.08 - 0.24 Hz, red, dependent of velocity), corrective steering movements (0.25 - 1 Hz, green) and the force perturbation signal (1.25 - 20 Hz). Corrective movements are clearly present for curvy road conditions. The frequencies above 0.25 Hz were amplified by 100 for the sake of clarity (road frequency responses have much greater power) for the figures only. (c): Boxplot of three-way interaction effect between preview ('LP' is low preview, 'MP' is medium preview' and 'HP' is high preview), tolerance ('tol') and velocity ('vel') on corrective steering PSD as a percentage of the total steering PSD (i.e., the percentage of the surface under the blue line at the green part with respect to the surface under the blue line at the red and green part combined.

Admittance analysis Figure 3-3 presents the spectral and ARMAX estimation of the gain and phase of the admittance of one typical subject performing the task in one of the conditions, i.e., for high preview, high tolerance and low velocity.
Two subjects returned low VAF values (VAF $>$ 40%) throughout the entire condition set. These subjects were removed from the dataset after a normality test of the obtained VAFs. For the remainder of the population (n = 16) relatively high VAFs were obtained (VAF $>$ 70%; see Figure 3-4b).

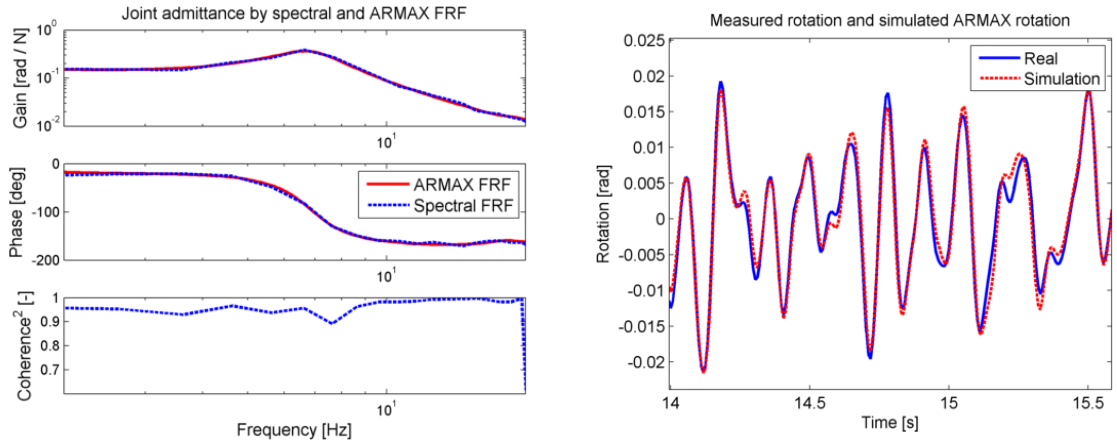

Figure 3-3: (a) Example of joint admittance of a typical subject. The magnitude (top panel), phase (middle panel) and coherence (lower panel) for the spectral and the ARMAX FRF are shown. (b) A 1.5-s example of the position response of the ARMAX model versus the measured position output for one of the conditions for a typical subject.

Preview ($F(2, 30) = 8.13$, $p = 0.002$, $\eta_p^2 = .35$) and tolerance ($F(1.31, 19.64) = 21.10$, $p < 0.001$, $\eta_p^2 = .58$) showed significant main effects on admittance. Furthermore a three-way interaction effect between preview, tolerance and velocity was found ($F(8, 120) = 3.38$, $p = 0.002$, $\eta_p^2 = .18$).
Figure 3-4a shows a boxplot of the three-way interaction of preview, tolerance and velocity on admittance. From the figure it is clear that admittance increased for increases in tolerance. Admittance decreased for increasing preview for both medium and high tolerance in combination with high velocity. Increases in velocity appear to decrease admittance for medium tolerance in combination with high preview and for high tolerance in combination with medium and high preview. Furthermore, for low tolerance it is shown that admittance was higher for medium velocity than for low and high velocity. Finally, admittance was lowest for the most difficult condition (low preview, low tolerance, high velocity). The easiest condition (high preview, high tolerance, low velocity), among two other conditions, returned the highest admittance.

3-1-3 Parameter Estimation

Effects were found on the intrinsic muscle damping (b) and stiffness (k), the proprioceptive velocity feedback gain (k_v) and the visual position feedback gain (k_{vis})), which are presented in Figure 3-5.
SEM values were rather low (<1) for all parameters apart from kv ($1 < SEM_{k_v} < 3$; see Figure 3-5e). As expected, no statistical differences were found for the wrist inertia (I_{wr}, $M = 0.0049$ $[kg/m_2]$) and the proprioceptive neural time delay (τ_{ms}, $M = 0.077$ $[s]$, $SD = 0.030$ $[s]$). The visual neural time delay (τ_{vis}) failed the Kolmogorov-Smirnov normality test on all conditions due to non-normal distributions and a large spread of the data (see Figure 3-5f), since many of the parameter estimations converged to the boundary values of the optimization set (lower boundary: 0.08 s, upper boundary: 0.35 s).

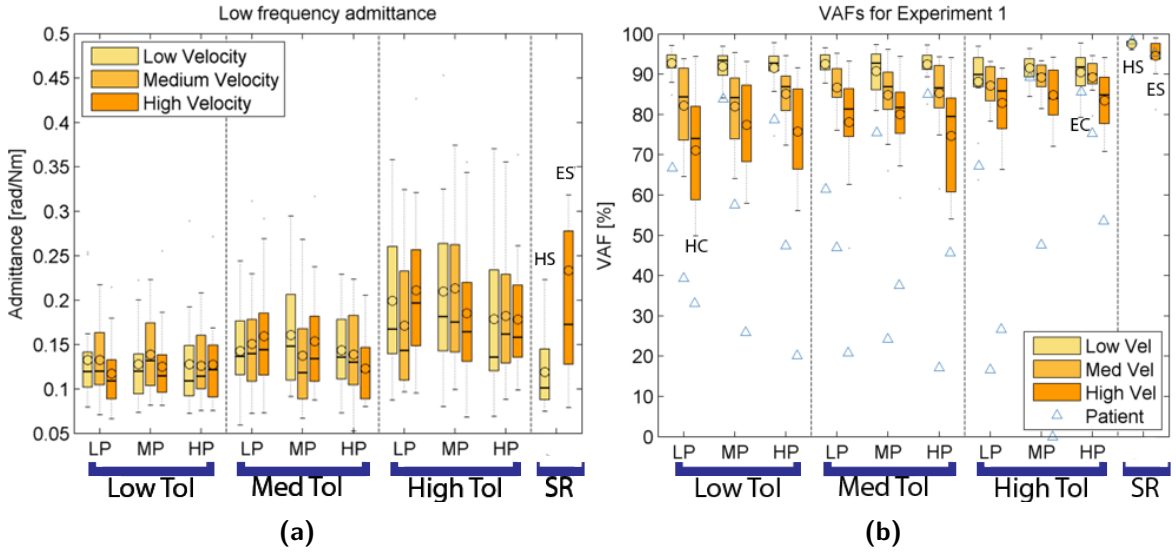

Figure 3-4: (a): A boxplot of the three-way interaction effect between preview, tolerance and velocity on the admittance and (b): the calculated VAFs for experiment 1 over all conditions, for n = 16 subjects and patient 2 (triangles). Preview was presented as 'LP' (low preview), 'MP' (medium preview) and 'HP' (high preview). Tolerance was presented as 'low tol' (low tolerance), 'med tol' (medium tolerance) and 'high tol' (high tolerance). In the boxplots, the stripe (-) describes the median and the circle (∘) the mean value.

Intrinsic muscle damping Main effects of tolerance ($F(2,30) = 8.80$, $p = 0.001$, $\eta_p^2 = .37$) and velocity ($F(2,30) = 17.14$, $p \leq 0.001$, $\eta_p^2 = .53$) and an interaction effect between tolerance and velocity ($F(2.75, 41.27) = 3.89$, $p = 0.018$, $\eta_p^2 = .21$) were found (see Figure 3-5a). Post hoc analysis of this interaction revealed that b increased for an increase in velocity, solely for medium and low tolerances, where effects were more pronounced for low tolerance.

Intrinsic muscle stiffness Main effects were found for tolerance ($F(1.45, 21.69) = 19.77$, $p \leq 0.001$, $\eta_p^2 = .57$) and preview ($F(2,30) = 6.37$, $p = 0.012$, $\eta_p^2 = .26$) on muscle stiffness (see Figure 3-5b). Post hoc analyses revealed significant differences between all three tolerance levels (low-medium $p < 0.05$, low-high $p < 0.01$ and medium-high $p < 0.01$). k was high for low tolerance and decreased for medium and high tolerance. Furthermore, a significant higher stiffness was found for a low preview with respect to medium preview ($p < 0.05$).

Reflexive velocity feedback gain A main effect of tolerance ($F(1.70, 25.47) = 9.64$, $p = 0.001$, $\eta_p^2 = .39$) on k_v was found, which was complemented by an interaction effect between velocity and tolerance ($F(1.83, 27.48) = 4.78$, $p = 0.019$, $\eta_p^2 = .24$). k_v became more negative for decreases in tolerance, but only at the highest velocity (Figure 3-5c).

Visual position feedback gain Main effects on k_{vis} were found for velocity ($F(2,30) = 14.81$, $p \leq 0.001$, $\eta_p^2 = .50$) and tolerance ($F(2,30) = 6.37$, $p = 0.005$, $\eta_p^2 = .30$). Post hoc analyses revealed a significantly higher k_{vis} for a high velocity with respect to a low velocity ($p < 0.05$). Furthermore a significantly higher k_{vis} was found for low tolerance with respect to medium

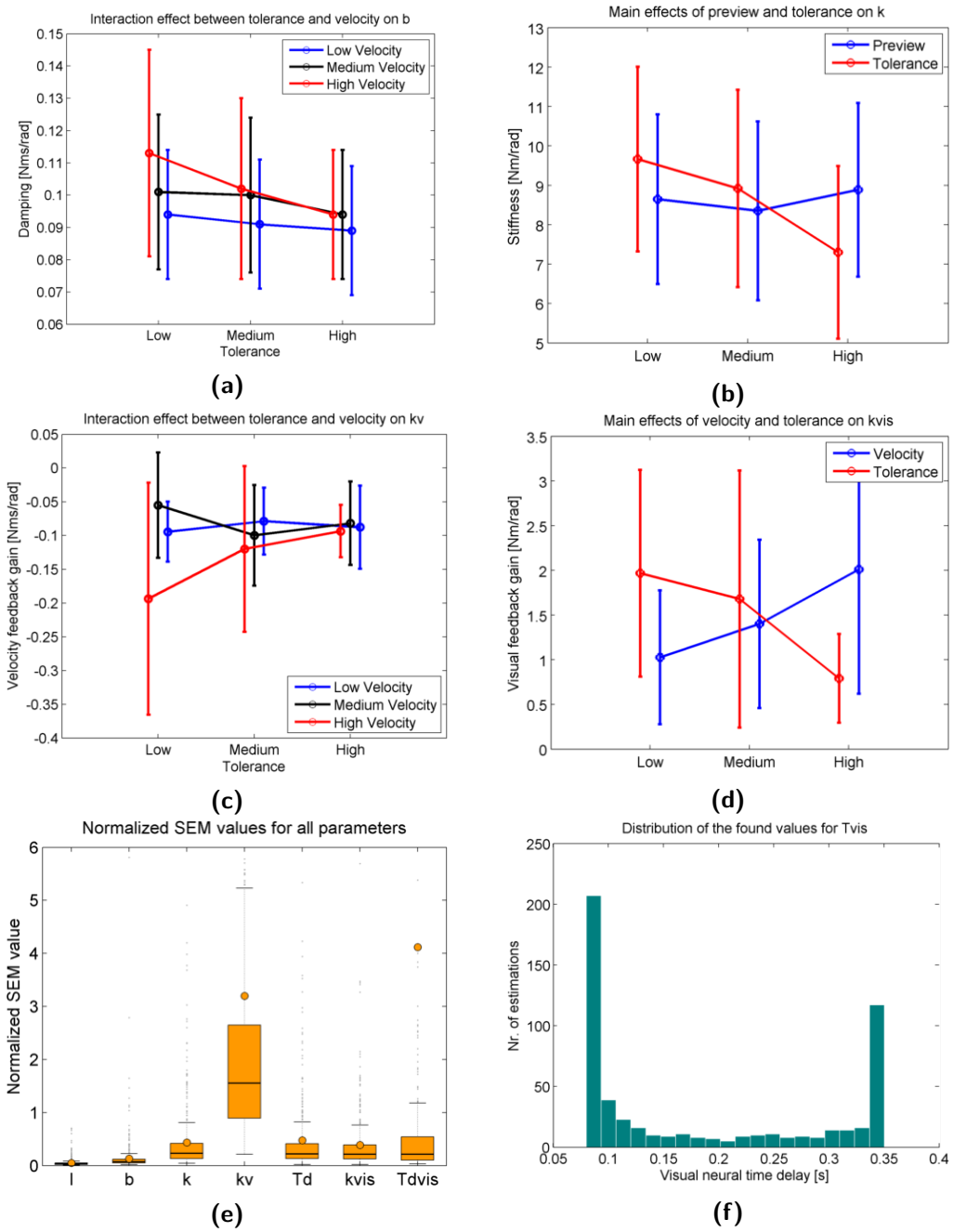

Figure 3-5: Results of neuromuscular parameter estimations. (a) to (d): Effects of all conditions on the neuromuscular parameters: muscle damping (b) and stiffness (k), reflexive velocity feedback gain (k_v) and visual position feedback gain (k_{vis}). (a) and (c) present the interaction effects of velocity and tolerance on b and k_v, respectively. (b) and (d) present the condition main effects on k (preview and tolerance) and k_{vis} (tolerance and velocity), respectively. (e): A boxplot of the found SEM values of all parameters over all conditions for n = 16 subjects. (f): A histogram of the results for τ_{vis}, representing all (432) estimations (16 subjects, 27 conditions). The circles and the errorbars describe the means and SDs, respectively.

Table 3-1: Results of the TV analysis for k for 10 subjects. The values describe the control change threshold time (T_{th}; i.e., the time from the start of the transition after which k changes more than the SD with respect to its mean value in HC), the control change magnitude (M; i.e., the change in k from HC to EC) and the control change slope (C; i.e., the tangent of k at the observed control change threshold time). Minus sign (-) denotes that no control change could be found.

	T_{th}	[s]		M	[Nm/rad]		C	[Nms/rad]	
Subject \ T_w (s)	2 s	4 s	8 s	2 s	4 s	8 s	2 s	4 s	8 s
1	9	9	8	1.85	1.20	2.00	-0.45	-0.42	-0.21
2	13	8	6	3.72	3.87	4.76	-0.45	-0.40	-0.14
3	3	2	1	2.32	2.57	2.47	-0.48	-0.28	-0.14
4	13	14	14	0.87	-0.30	-0.04	-0.23	-0.18	-0.31
5	7	8	7	2.53	2.49	2.69	-0.43	-0.40	-0.34
6	2	3	3	12.04	12.42	11.64	-0.77	-0.79	-0.77
7	19	13	13	2.40	2.84	3.20	-0.19	-0.12	-0.14
8	-	7	6	0.80	0.95	1.07	-	-0.07	-0.09
9	15	12	13	3.36	3.89	3.56	-0.21	-0.19	-0.29
10	14	11	10	1.14	1.72	1.52	-0.08	-0.14	-0.22

tolerance ($p < 0.05$) and low tolerance ($p < 0.001$), and between medium and high tolerance ($p < 0.05$) (Figure 3-5d).

3-1-4 Time Variant Results

Test Case: Hard (HC) to Easy (EC) 10 subjects returned sufficient ARMAX model estimations (VAF $\geq$ 70 %; Figure 3-7b) for both HC and EC. SEM values for k were low (<1). The results of a typical subject are illustrated in Figure 3-6. Time window length had a substantial effect on the variability of the response of k. The results of all 10 subjects for $t_w = 4$ s are demonstrated in Figure 3-6d and the observed control change threshold times, magnitudes and slopes are presented in Table 3-1. Responses of b, k_v and k_{vis} showed too high variability for all three time windows and were therefore not assessed.

The greater part of the subjects responded rather late to the condition change; 5 out of 10 subjects showed changes in stiffness *after* the transition was completed. Control change magnitudes (M) varied substantially between subjects, whereby one subject showed a relatively large decrease (12.04 Nm/rad). Results varied between the analyzed time windows, due to the averaging effect of higher time windows (i.e., for $T_w = 2$ s k is estimated and averaged over 2 seconds and for $T_w = 8$ s k is estimated and averaged over 8 s).

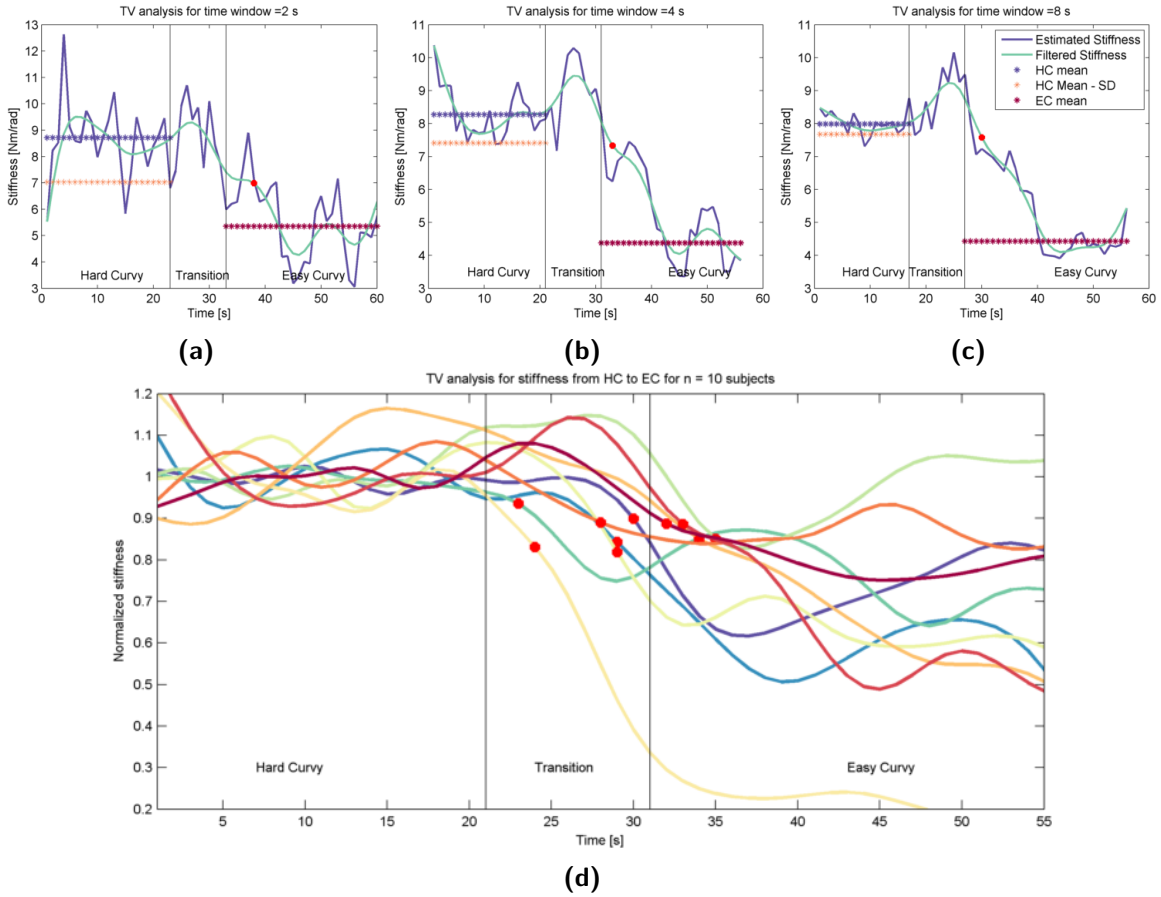

Figure 3-6: The response for k for a typical subject from HC to EC for a time window of (a) 2 s, (b) 4s and (c) 8s. The low time window (a) results in high variability, whereas the variability is reduced due to averaging for higher time windows (c). (d) describes the results for $T_w = 4$ s for all subjects. The red dot denotes the observed control change threshold time. The transition area is defined by the two vertical black lines.

Road Influence

Validity Figure 3-7 illustrates the found coherences of all test subjects of a TV analysis on both HC, EC, HS and HE with $T_w = 4$s. Coherences for HS and ES were high over the total frequency bandwidth. In contrary, coherences for HC and EC decreased for decreasing frequency, which predominantly affected 2 to 6 Hz.
VAFs were high for HS and ES, somewhat lower for EC and low for HC (Figure 3-7b). SEMS for EC, HS and ES, as compared to HC, were remarkably lower for k, k_v and k_{vis} but, overall, were comparable with the found SEMs of Section 3-1-2 (see Figure 3-7d).

Road-Parameter cross correlation Figure 3-7a illustrates a boxplot for all found cross correlations between the road and the seven model parameters. Cross correlations were moderate for EC and low for HC.

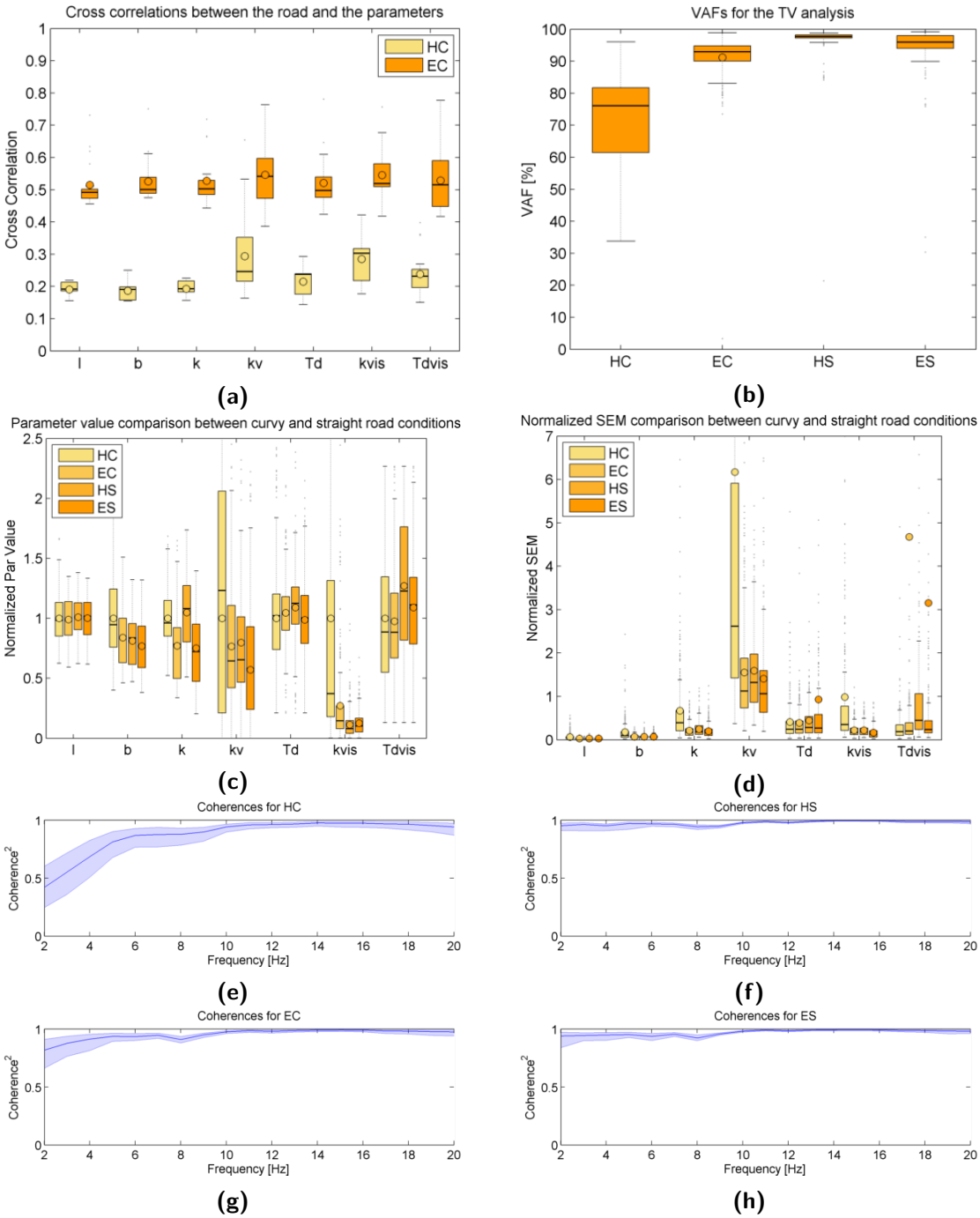

Figure 3-7: Analysis of the cross correlations of the road position with the model parameters (a), the obtained VAFs (b), obtained model parameters (normalized to the values found for HC) (c) SEM values (d) and coherences (e, f, g and h) for a TV analysis with $T_w = 4$s for HC, EC, HS and ES. All analyses were done on n = 16 subjects. The first four figures denote the box plots with 25th (Q1) and 75th (Q3) percentiles. Coherence plots describe the mean (blue line) and SD (shaded area) of the total (n = 16) population.

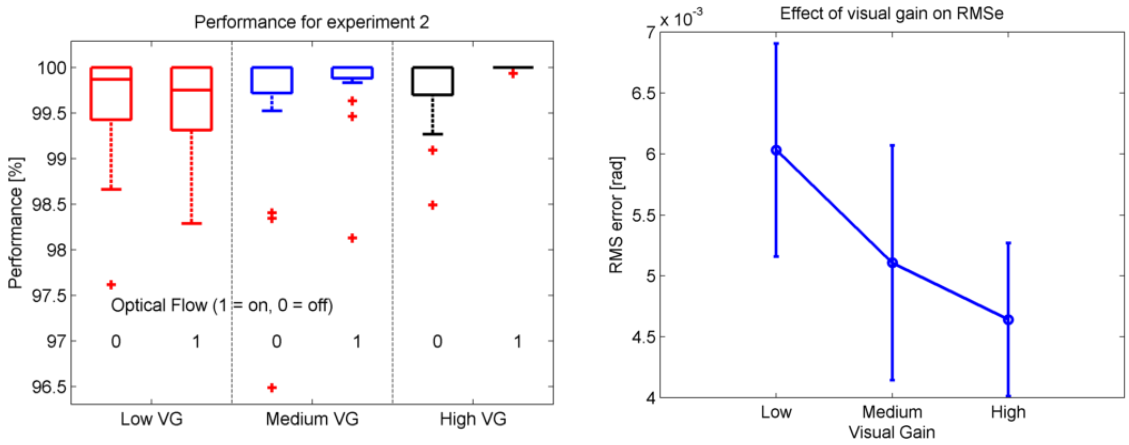

Figure 3-8: (a): The task performance as a function of low, medium and high visual gain (VG) and optical flow. Box plots are described by median, 25th (Q1) and 75th (Q3) percentiles. (b): The effect of visual gain on RMSe. Circles denote mean value of the total population (n = 16), errorbars denote SD.

3-2 Experiment 2

3-2-1 Time Domain Analysis

Performance As expected, subjects performed equally well for all six conditions (see Figure 3-8a); no significant differences could be found. However, Figure 3-8a does show indications of overall better performance for increases in visual gain (VG), as well as for optical flow (OF; i.e., the presence of the tunnel) in medium and high VG.

RMS error Statistically significant main effects were found for VG ($F(2,34) = 188.72$, $p < 0.001$, $\eta_p^2 = .57$) on RMSe. Post hoc analyses (Figure 3-8b) showed a significant higher RMSe for low VG with respect to medium VG ($p = 0.007$) and high VG ($p < 0.001$), whereas RMSe was also significantly higher for medium VG than for high VG ($p = 0.043$).

EMG Two subjects were extracted from the population due to extremely high EMG values ($> EMG_{MVC}$) for every condition. Significant main effects for OF were found for the ECR muscle ($F(1,15) = 5.48$, $p = 0.033$, $\eta_p^2 = .016$), where EMG recordings were higher without tunnel than with tunnel (Figure 3-10b).
For FCR EMG, one subject was extracted from the test population due to extremely high EMG values. No significant main effects were found, despite a non-significant effect for VG ($F(2,30) = 2.91$, $p = 0.07$, $\eta_p^2 = .16$). Furthermore, the significant effect for OF at the ECR muscle was not found for the FCR muscle, apart from an equivalent trend ($p = 0.16$).

Steering delay and anticipation Solely steering anticipation was found (see Figure 3-9). VG had a pronounced effect on steering anticipation ($F(2,34) = 188.72$, $p < 0.001$, $\eta_p^2 = .92$),

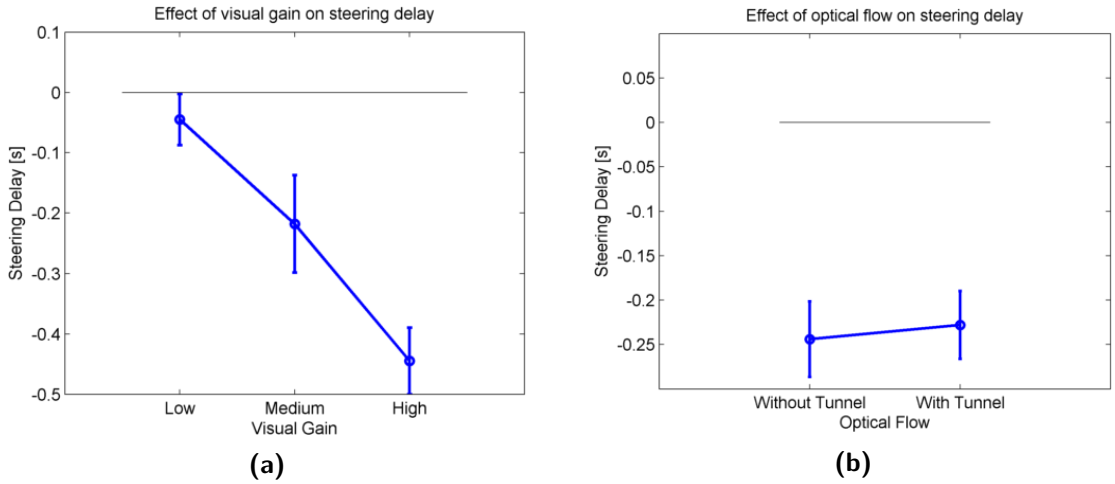

Figure 3-9: Observed steering delays due to changes in (a) visual gain and (b) optical flow. Circles denote mean value of the total population (n = 18), errorbars denote SD.

where an increase in VG increased anticipatory steering (i.e., negative time delays). Post hoc analyses showed significantly higher anticipatory steering for high VG than for medium ($p < 0.001$) and low VG ($p < 0.001$), and medium VG returned significantly higher anticipatory steering than low VG ($p < 0.001$). Furthermore, a non-significant higher steering anticipation was found for with tunnel ($F(1, 17) = 4.32$, $p = 0.053$, $\eta_p^2 = .20$) than without tunnel (Figure 3-9b).

3-2-2 Frequency Domain Analysis

Corrective steering PSD The main effects for visual gain ($F(1.14, 19.36) = 45.84$, $p < 0.001$, $\eta_p^2 = .73$) and optical flow ($F(1, 17) = 8.88$, $p = 0.008$, $\eta_p^2 = .34$) were complemented by an interaction effect between visual gain and optical flow ($F(1.35, 22.95) = 3.85$, $p < 0.031$, $\eta_p^2 = .19$). Figure 3-10a illustrates that corrective steering PSD mainly increased due to increases in visual gain, especially in combination with the presence of a tunnel.

Admittance Analysis VAFs were high for all analyses ($> 90\%$), where VAFs were somewhat lower for low VG with respect to medium and high VG (see Figure 3-10e).
Main effects were found of VG on admittance ($F(2, 34) = 3.81$, $p = 0.032$, $\eta_p^2 = .18$). Post hoc analyses revealed a significant higher admittance for a high VG with respect to low VG ($p = 0.046$).

3-2-3 Parameter Estimation

Stiffness No significant effects were found apart from VG on k ($F(2, 34) = 4.77$, $p = 0.015$, $\eta_p^2 = .22$). Post hoc analysis revealed a higher k for high VG as compared to low VG (Figure 3-10d). τ_{vis} was distributed in the same manner as in experiment 1.

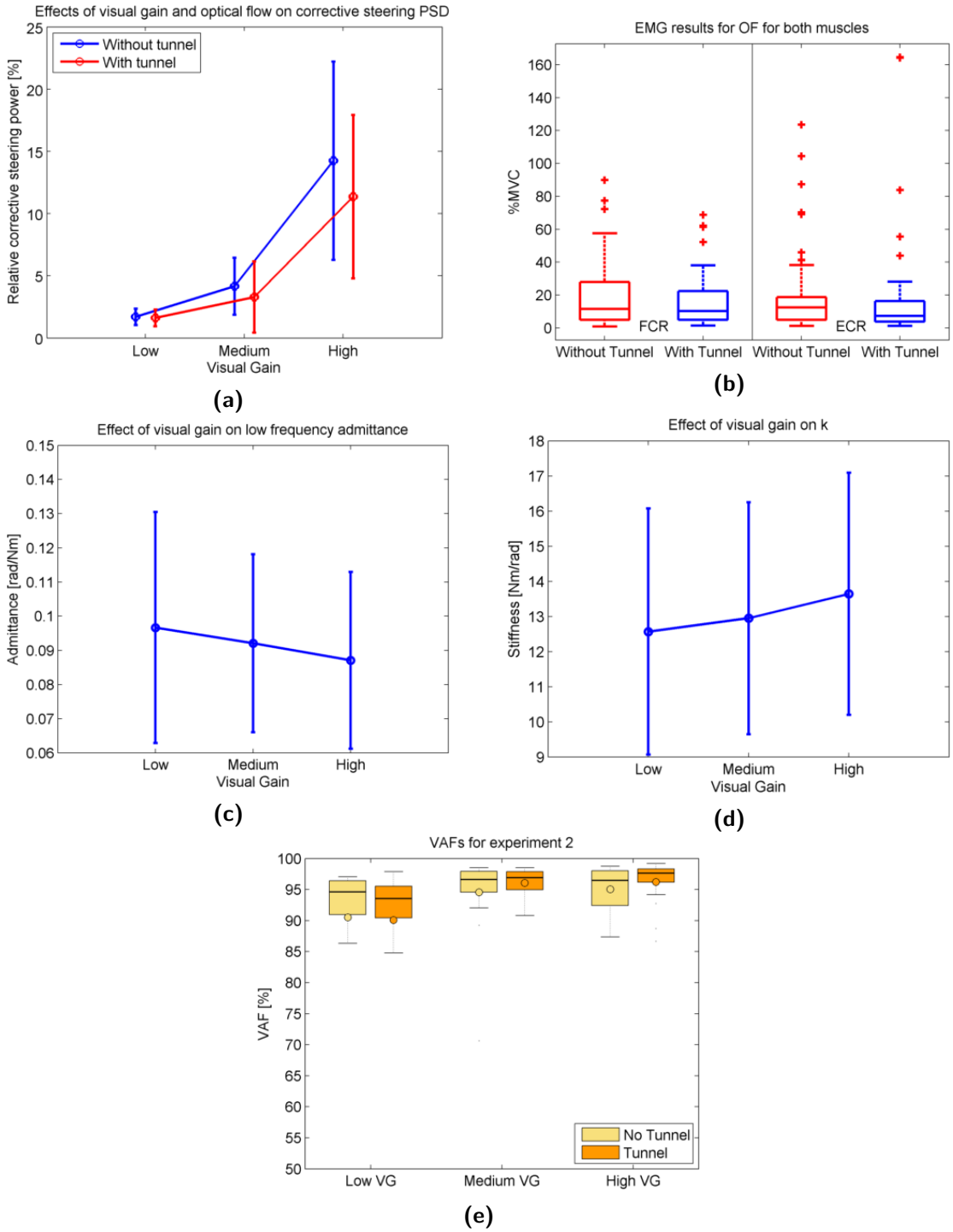

Figure 3-10: (a): Interaction effect of OF and VG on corrective steering PSD. (b): The observed main effect of OF on FCR and ECR EMG. c: Main effect of VG on admittance. (d): Main effect of VG on k. (e): Calculated VAFs for experiment 2. Circles denote mean value of the total population (n = 18), errorbars denote SD. Box plots are described by median, 25th (Q1) and 75th (Q3) percentiles.

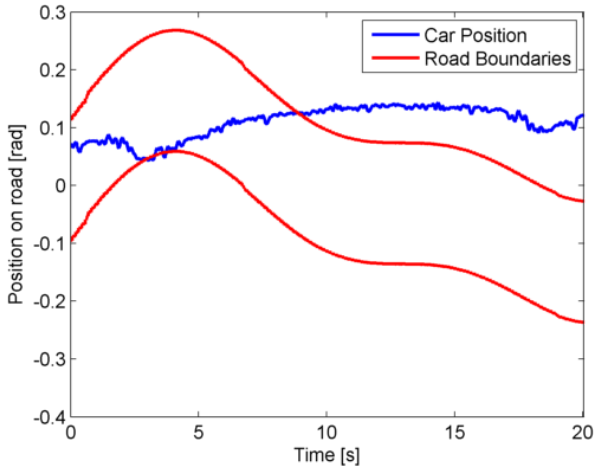

Figure 3-11: An example of the car position with respect to the boundaries of the road for a typical condition for patient 2. Patient 2 was unable to extend the wrist and thus failed to properly follow the road.

3-3 Feasibility Study

Patient 1 successfully accomplished the protocol. Patient 2 was unable to perform the task due to spasticity of the arm muscles, which allowed flexion movements but obstructed extension movements (see Figure 3-11).

Performance Performance was remarkably lower for patient 2 than for the rest of the test population (see Figure 3-1a). Performance was especially affected by increasing levels of velocity and decreasing levels of tolerance.

VAFs Figure 3-4b illustrates the obtained VAFs for all conditions of experiment 1 for the total test population including patient 2 (denoted by blue dots). VAFs were predominantly low ($< 70\%$) for conditions with medium or high velocity and medium or low preview, with respect to the healthy subjects. In contrast, VAFs for the straight road conditions (HS and ES) were comparable to those of the healthy subjects ($> 90\%$).

Main conclusions from questionnaires Both patients found the task motivating and amusing, were not distracted and did not experience any pain or severe mental stress. Logically, patient 2 indicated that fulfillment of the task was impossible. Lastly, task performance feedback should have been adjusted to the capabilities of patients.

Chapter 4

Discussion

The main goal of this study was to investigate if and how changes in visual feedback affect motor control in a continuous tracking task. The effects of task demand by means of changes in preview, tolerance and velocity, and the effects of changes in visual properties (i.e., visual gain and optical flow) were analyzed in the time domain (e.g., performance, control effort) and in the frequency domain (e.g., ,steering power spectral densities (PSD), admittances and parameter model fits). A summary of the results is presented in Table 4-1. Limitations and recommendation with respect to the present study is described in the last paragraph.

Experiment 1: Effects of task demands In experiment 1, task demands were varied by combinations of tolerance, velocity and preview. Outcome parameters were most sensitive to changes in tolerance. Therefore, tolerance will be discussed first, after which velocity and preview will be discussed.
Outcome parameters were most sensitive to changes in tolerance (see Table 4-1). Firstly, tolerance decrease (i.e., narrower road) was associated with decreased performance, decreased RMSe and reduced admittance, especially in combination with high velocity and/or low preview, which was consistent with a previous study (Selen et al., 2006a). It indicates that tracking errors were predominantly caused by higher demands on task precision and movement frequency, which both contributed to higher control effort, especially in combination with limited future road information. Secondly, tolerance decrease evoked increases in stiffness, and in combination with increased velocity, tolerance decrease invoked increases in damping. Increases in stiffness can be explained by the fact that higher muscle forces, caused by co-contraction (which could not be confirmed by the recorded EMG data) or by higher accelerations as a result of a higher movement frequency, suppressed force perturbations to retain task precision on a narrower road. However, joint motion can solely be achieved by differences in muscle force between the agonist and antagonist muscle. This suggests that many possible combinations of agonist/antagonist contractions can be evoked to rotate the wrist. For instance, flexion movements could be mediated by reduced antagonist contraction or increased agonist contraction (with respect to the co-contraction level). So why did damping increase and remained stiffness unaffected for increased velocity? Selen et al. (2006a)

hypothesized that higher movement frequencies require larger propelling forces, which result in greater neuromuscular noise, requiring increased muscle stiffness and damping to attain the required accuracy. Forces however, are not dependent of velocity but of acceleration, which explains that Selen et al. (2006a) could not find increased stiffness and damping at peak velocities. A more consistent explanation therefore is that the agonist and the antagonist muscles alternated contraction levels between steering actions (i.e., flexion movements increase contraction in the FCR (flexor muscle) and decrease contraction in the ECR (extensor muscle) and vice versa) and peak velocity levels (i.e., high movement displacements, low co-contraction) and that damping increased as a result of muscle lengthening (i.e., muscle force-velocity relation; Winters and Stark (1985)). This would allow joint motion and retain an increased total stiffness and damping to attend to decreased tolerance. Finally, tolerance decreases were associated with larger negative values of k_v in combination with high velocity, and increases in k_{vis}. The findings demonstrate that higher demands on task precision by visual feedback manipulation can be employed to evoke changes in these feedback mechanisms. Velocity increases were associated with decreased performance, higher power in the corrective steering power spectral density (PSD) and increases in b and k_{vis}, especially in combination with low tolerance. The results indicate that velocity was the main cause to evoke steering corrections on top of the low frequent road tracking movements. This corresponded to larger tracking errors, which were mainly corrected for by the previously discussed intrinsic mechanisms and the visual feedback gain. The findings suggest that subjects put more visual attention to the deviations of the car position when task execution became particularly critical, going hand in hand with the observed increased steering delays. In specific, steering delay increased (positively) for critical (i.e, high task demand) conditions (high velocity, low tolerance) and became negative for non-critical task conditions (low velocity, high tolerance). It can therefore be concluded that in non-critical task conditions visual feedback is mainly used to anticipate to future situations and that if task performance is about to be at risk, visual attention switches to the car position and the feedback gain is increased.
Low preview was associate with increased stiffness and delayed steering, whereas high preview in combination with high tolerance resulted in anticipatory steering (i.e., negative time delay). These results indicate that subjects anticipated to the course of a wide road without view obstruction, proving that preview was thé dependent factor for the application of anticipatory control, provided that task demands allowed for such behavior. The increased stiffness in case of low preview might be explained by the idea that the lack of future road information increased the uncertainty of the visual feedback, which made the predictions unreliable (Bays and Wolpert, 2007; Wolpert and Ghahramani, 2000). This may have resulted in higher tracking errors, which can be suppressed by an increase in muscle stiffness. It could be argued that the fairly predictable road course, which was composed of merely two sinusoids, allowed subjects to memorize the track and not be influenced by the low preview. However, the increased tracking errors indicate that subjects needed online visual information to anticipate to the road. Therefore, it is likely that co-contraction was increased when visual information was limited to retain task performance.

Experiment 2: Effects of visual properties Visual gain increases were associated with decreases in RMSe and admittance, and increases in performance (although non-significant), which confirms findings of previous studies where the error of force control (i.e., 'keep force

at a constant level'; Hong and Newell (2008)) or position control (i.e., keep position constant; Beuter et al. (1995)) was visually amplified. Furthermore, visual gain increases resulted in increases in intrinsic stiffness and anticipatory steering and decreases in corrective steering movement PSD.
Firstly, the results illustrate that, although task demands remained the same, motor control was adapted to changes in visual feedback. Secondly, the increased stiffness suggests that subjects applied higher levels of muscle co-contraction to minimize (amplified) deviations due to external force perturbations, although this could not be confirmed by results of the EMG analysis. Thirdly, it can be concluded that the level of anticipation was not only determined by preview but also by visual gain. An increase in visual gain resulted in a decrease in RMSe, which provided a better estimation of the car position relative to the road, since deviations were minimized. It can therefore be speculated that increased visual gain resulted in increased governed control behavior, which allowed subjects to put more attention to the future road course, thereby applying increased levels of anticipatory control. Finally, it is speculated that high frequent movements were emphasized by increased visual gain. This resulted in a more substantial reaction to these frequencies, which explains the observed increase of corrective steering PSD. It could therefore be that increases in visual gain increased the level of intermittent control.
The presence of a tunnel was associated with decreases in ECR EMG (significant) and FCR EMG (non-significant) and improved task performance (which agrees with findings by Berntsen et al. (2005); Johnston et al. (1973)). In conditions with high visual gain, presence of tunnel was also associated with increased corrective steering PSD in combination with high visual gain. Possibly, optical flow provided a guidance function, rather than a stressing function as was hypothesized. In specific, optical flow may have increased the reliability of visual information by providing more information about the velocity, thereby making future predictions about the state of the environment more reliable (Wolpert and Ghahramani, 2000), which in turn may have resulted in higher performance (Figure 3-8a) and lower muscle activity (Figure 3-10b). On the one hand, increased corrective steering PSD might reflect increased task demands, in which subjects continuously compensate tracking errors by applying high frequent corrective movements. On the other hand, it may indicate an improved use of visual feedback to tracking execution, whereby low frequent corrective movements are perfectly timed to enhance tracking performance (Miall et al., 1993). To this respect, the latter explanation seems more feasible, because improvement of performance was observed. However, to discriminate between these control strategies, a study of the main corrective steering frequency should be conducted to determine the level of intermittent control.

Time variant analysis The LTI approach to estimate time variant (TV) behavior worked notably well for straight road conditions. The results demonstrate that an analysis window of merely 2 seconds provided high VAFs, which suggests that the estimated ARMAX models described the measured behavior well. However, for the hard curvy (HC) condition, low frequent coherence dropped significantly and ARMAX model estimations were rather poor. Consequently, this poses limitations to the usability of the method in active steering tasks. Furthermore, due to parameter outcome variability as a result of steering actions, it was difficult to distinguish parameter variation from a potential control change. Increased time windows resulted in more smooth responses at the cost of time resolution. The analysis therefore poses a trade-off effect, which should be taken into account for the analysis of

Table 4-1: A summary of the found results for experiment 1 and 2. Increases of the outcome parameters (first column) are denoted by a plus (+), decreases are denoted by a minus (-). The presence of an interaction effect were highlighted by a cross (x). Empty cells means that no effect was found for the corresponding condition.

	Prev low	high	Tol low	high	Vel low	high	VG low	high	OF on	off	Prev Vel	Prev Tol	Vel Tol
Performance [a]			-	+	+	-	-	+	-	+			x
RMSe			-	+			+	-				x	x
Steering delay [b]	+	-	+	-			+	-				x	
EMG_{fl}													
EMG_{ex}									-	+			
Corrective steering PSD			-	+	+	-	+	-					x
Admittance	-	+	-	+			+	-			x	x	x
b			+	-	-	+							x
k	+	-	+	-			-	+					
k_v [c]			-	+									x
k_{vis}			+	-	-	+							

[a] Results were non-significant.

[b] Minus (-) denotes steering anticipation, plus (+) denotes steering delay.

[c] In the case of k_v a minus sign denotes a decrease in value as well as an increase in magnitude, due to the negative nature of k_v.

interest. It was expected that model parameters were predominantly sensitive to the road in the HC condition and to a far lesser extent to the easy curvy (EC) condition. However, cross-correlations between the road and the outcome parameters revealed exactly the opposite. This can possibly be explained by the fact that subjects were better in fluently following the road in EC, while they applied a more aggressive steering style for HC resulting in more corrective steering movements (hence the low coherences at low frequencies and increased corrective steering PSD (Table 4-1)). Moreover, observed steering responses above 1 Hz were likely attributable to resolute wrist movements rather than controlled steering behavior (Miall and Jackson, 2006).

Physiology of feedback parameters The results clearly indicate that manipulation of visual feedback evoked changes in reflexive feedback mechanisms. The found values for k_v however, directly pose questions about its size, sign and origin.

The low values are presumably attributable to suppressed reflexive feedback to retain stability, in the presence of force perturbations at the eigenfrequency of the wrist joint (van der Helm et al., 2002). A previous study (Mugge et al., 2007) showed that this suppression effect can be resolved by applying reduced power to the higher frequencies, which enables identification over the full admittance range with high coherence, while evoking control behavior that is adapted to low perturbation bandwidths.

The negative nature of k_v indicates that the found feedback mechanism was inhibitory, while k_v was expected to be excitatory. Reflexive velocity feedback, however, has been found to become negative for high values of relative damping (increased negative environmental damping; de Vlugt et al. (2002)) and in position tasks (Mugge et al., 2010). In the present study, increased negative values were found for high task demand conditions (similar to position task) and particularly low negative values were found for low task demand conditions (similar

to relax task), which correspond to findings of Mugge et al. (2010) for position and relax tasks respectively.
Studies on the cat suggest that negative reflexive gains may arise from presynaptic inhibition resulting in an inhibitory effect to the Ia afferent input (Jankowska and McCrea (1983); muscle length change rate) and an inhibitory effect on Ib afferent input (muscle force) due to shared interneural circuits (Brink et al., 1983). In humans, Mugge et al. (2010) showed that slightly inhibitory velocity feedback has a stabilizing effect near the GTO's eigen-frequency, allowing more excitatory GTO feedback. However, in the present study, GTO (force) feedback showed to have a poor contribution to the model fit, which suggests that reflexive inhibition was not a result of force feedback mechanisms. More importantly, the observed time delays ($\approx$ 70 ms) suggest long-latency (M2) rather than short-latency responses (M1; $\approx$ 30 ms) (Schmidt, 2008). In contrast to M1 responses, M2 responses are mediated by the spinal cord *and the cortex* and are known to incorporate more sensory information and to be more flexible to task instruction, which suggest that M2 responses may have been modulated by supraspinal steering commands (give way to perturbations in the extension direction for extension movements and vice versa). It could therefore be that M1 responses were suppressed as a result of the force perturbations and that M2 responses were used to *allow* steering actions. Evidently, this notion requires additional research. It is important to note that k_v was essential for a proper model fit (Appendix C-6), which emphasizes its contribution to the observed movement behavior.
Other than M1 and M2 responses, visual feedback may be processed by the so-called voluntary reaction-time response (M3, 120 - 180 ms), which is mediated by the cortex and the spinal cord (Schmidt, 2008). It is certain that the observed values for k_{vis} were *not* caused by proprioceptive feedback mechanisms, since visualizations from motor input (at the WA) were delayed by over 200 ms (by a hardware delay (Appendix C-1) and a first order visual filter), which was compensated for in the parameter model (Appendix C-7). Due to the slow nature of visual feedback, it can solely bring about changes in low frequent behavior, which clarifies why the addition of visual feedback improved the parameter fit only marginally. However, the relatively low SEM values for k_{vis} and τ_{vis} suggest a reliable contribution of these parameters to the model fit. Illustrative is the large variation between the observed values of τ_{vis} (Figure 3-5f), which might suggest that one part can be attributed to M3 responses and that the other part is likely to originate from supraspinal (i.e., voluntary) steering corrections. Alternatively, the large variation might be due to a high intra-subject variability or to the fact that visual feedback actions are typical of time variant control behavior. The latter could have resulted in local minima in the optimization landscape, which indicates that the parameters have contributed mathematically to the defined model but do not represent the correct parameter behavior. Although this could be tested by simulation of the model with the obtained parameters, such analyses fell out of the scope of this study.

Feasibility study Feasibility of the protocol was assessed by subject experience (i.e., by questionnaires), task performance and data validation (VAFs). Patient 2 suffered from severe spastic muscles, which only allowed flexion movements. For patient 1, task execution and performance seemed to be sufficient during both experiments. However, data analysis revealed severely lower performance (Figure 3-1a) and lower VAFs with respect to the healthy subjects, especially for low tolerance and high velocity conditions. It can be concluded that low VAFs

were not necessarily caused by high task demands, but rather by the inability of executing coordinated steering movements, since VAFs were low for both high demanding and low demanding conditions. Therefore, no conclusions could be made with respect to changes in control behavior. However, the patient performed surprisingly well for the straight road conditions in terms of VAF (VAFs $> 95\%$; Figure 3-4b), which suggests that the protocol is feasible, provided that patients are not subjected to coordinated movements.

Recommendations for future research Firstly, the limitations of the present study are discussed and potential improvements are suggested. Thereupon, the improvements will be included into a recommendation to improve and extend the present study.
Wristalyzer (WA) - Virtual environment (VE) coupling. The coupling between the WA and the VE has been a critical limitating factor in the development of the protocol. It resulted in low data sampling rates (initially < 30 Hz, eventually for the experiments ≈ 100 Hz) and a high time delay between movements of the WA and visualizations in the virtual environment (≈ 135 ms; for an explanation, see Appendix C-1). Presumably, these limitations were caused by a poor communication protocol between the WA and the VE computer, which was not improved during the course of the present study. High time delays pose immediate limitations to the potentially evoked steering intermittency of subjects (Section 3-1-2, Miall and Jackson (2006)), which is particularly undesirable in the study of dynamic behavior in tracking tasks. For future research, it is therefore recommended to ensure a minimal time delay in the mechanical - visual interaction.
Arm fixation. EMG was particularly influenced by external noise, such as steering behavior and limb movement, since the sensors were trapped between the arm and the arm fixation. It is advised to design a two-point fixation which firmly fixates the lower arm just before the wrist and at the elbow to prevent medial rotation movements, thereby leaving space for the placement of EMG electrodes.
Perturbation signal. The bandwidth and the power of the perturbation signal has a significant influence on the results and should therefore be designed carefully. In the present study the perturbation signal may have suppressed reflexive contributions due to the full power bandwidth. It is therefore advised to investigate the influence of the bandwidth on neuromuscular parameters by means of the reduced power method (Mugge et al., 2007). Furthermore, since wrist dynamics could be captured within the 2 - 20 Hz frequency bandwidth, low bandwidth frequencies (< 2 Hz) can be used to create a position forcing function, in order to study visual contribution to road anticipation according to methods described in Steen et al. (2011). However, it is advised to minimize road curvature, since active steering has shown to provide responses up to 5 Hz (see Figure 3-7) in the present study, when task demands are high.
Study proposal. It is recommended to employ the TV approach to a similar protocol comprising the assessment of reflex gain adaptation to changing environments (visually and/or mechanically) in e.g., position tasks, *with minimal steering.* Apart from the identification of neuromuscular parameters in constant environmental conditions, the TV approach will allow for identification during the actual adaptation of the underlying mechanisms, *in time.* This may provide insights in the adaptability of the imperative mechanisms that contribute to movement control in both healthy subjects and patients. To study the significance of the visual position feedback parameter, it would be valuable to include a condition in which the controlled variable (i.e., the car) suddenly disappears. Logically, it would be expected that visual position feedback contribution drops. Furthermore, the degree of anticipation to the

road could be validated by eye tracking equipment to validate findings which suggest anticipatory control behavior. Finally, in the case of an active steering task, it could be insightful to explore the potential of separately modeling the contribution of the agonist and the antagonist muscles. Subsequently, EMG data can be used to validate the results.

Chapter 5

Conclusions

This study investigated how changes in visual feedback, by variations in task demands and by changes in visual properties, affected task performance and control strategy in a continuous visuomotor tracking task. It is concluded that the imposed conditions had a substantial effect on both tracking performance and neuromuscular properties.

Firstly, tracking errors were predominantly caused by higher demands on task precision and movement frequency. This reflected in increased intrinsic stiffness and damping, increased visual position feedback, accompanied by slightly inhibitory reflexive feedback. Secondly, preview accounted for the degree of anticipation to the road, provided that task demands were low. Finally, an increase in visual gain increased task performance and RMSe, which reflected in an increase in stiffness, where optical flow tended to increase performance when visual gain was high.

The findings suggest that humans flexibly adapt their use of visual feedback between continuous feedback and intermittent feedback control, dependent of demands on task precision and movement frequency. Anticipatory feedback control was dependent on the amount of future task information available, but was suppressed by high task demands and increased when movements were visually amplified. Optical flow, which tended to increase task performance, may act as a velocity cue reliability optimizer, which guides controlled motor output to improve tracking performance.

LTI models can successfully be deployed for the analysis of TV control behavior in tracking tasks, provided that actual movement amplitudes are small. It is concluded that the discussed methods, both time invariant as time variant, yield potential in the identification of motor control adaptability and for the use in diagnostics of movement disorders. Finally, the protocol and the data analysis techniques were feasible for the measurement of stroke patients, provided that no coordinated steering movements were involved.

Appendix A

Information and Forms

A-1 Information letter to subjects

Informatie ten behoeve van het onderzoek: "NEURASV: Invloed van visuele informatie op het motorisch gedrag"

Geachte heer/mevrouw,

U ontvangt deze informatie omdat u gereageerd heeft op een oproep om als controlepersoon mee te doen aan een wetenschappelijk onderzoek naar nieuwe technieken voor het meten van bewegingssturing. Wij willen u hierbij nader informeren over dit onderzoek.

Achtergrond van het onderzoek
Op de afdelingen neurologie en revalidatie van het Leids Universitair Medisch Centrum (LUMC) wordt in samenwerking met de Technische Universiteit Delft onderzoek gedaan naar bewegingsstoornissen bij verschillende neurologische aandoeningen, zoals een beroerte of de Ziekte van Parkinson. De bewegingsproblemen bij deze aandoeningen kunnen verschillende oorzaken hebben: zijn het veranderingen in de spieren, gevoelsstoornissen, of veranderingen in de hersenen? Om te bepalen welke behandeling het meest geschikt is voor een bepaalde patient, is het van groot belang om te kunnen vaststellen waar precies het probleem zit. In de klinische praktijk is er grote behoefte aan meetinstrumenten die dit mogelijk maken.

Doel van het onderzoek
Het uiteindelijke doel van dit onderzoek is om de bewegingsproblemen van patiÃńnten beter in kaart te kunnen brengen en de onderliggende oorzaak van de bewegingsproblemen beter te kunnen begrijpen. Daartoe zal gebruik gemaakt worden van nieuwe technieken: een computergestuurde robot zal worden gecombineerd met een virtuele visuele omgeving. Om de mogelijkheden van deze technieken optimaal te kunnen benutten, is het van groot belang om

te weten hoe visuele informatie kan worden gebruikt bij het aansturen van bewegingen. Betere kennis over dit onderwerp kan aanknopingspunten bieden voor het ontwikkelen van een test voor het vaststellen van bewegingsproblemen bij patienten met neurologische aandoeningen.

Wat houdt deelname aan het onderzoek in?
Het onderzoek bestaat voor u uit:

1. Het invullen van enkele algemene vragen (zie bijlage) en vragen over handvoorkeur;
2. Het uitvoeren van bewegingstaken in het LUMC (duur ca. 60 minuten).

Voor deelname aan dit onderzoek ontvangt een bedankje in de vorm van een doos bonbons of een fles wijn; eventuele reiskosten worden vergoed op basis van de tarieven voor openbaar vervoer (2e klas).

Tijdens de metingen in het LUMC zit u in een comfortabele stoel en uw rechterarm rust op een steun. Op de huid van uw rechterarm zullen elektroden worden geplakt om de activiteit van uw armspieren te kunnen meten. Met uw hand houdt u een handvat vast, die u zelf kunt bewegen of die door een motortje kan worden bewogen. Tijdens de metingen kunt u uw hand niet zien.
Voor u is een groot televisiescherm geplaatst. Hierop zal een weg worden afgebeeld en een bolletje die de positie van uw hand weergeeft. U dient ervoor te zorgen dat het bolletje op de weg blijft door kleine bewegingen te maken met de hand.

Geen van de hier beschreven testen is pijnlijk. Het onderzoek in het LUMC duurt ca. 1 uur, waarvan 35 minuten voorbereiding en 25 minuten werkelijke meettijd.

Om aan dit onderzoek te kunnen deelnemen, dient u beide armen en handen onbelemmerd te kunnen gebruiken. U mag geen (ernstige) pijn in de armen of handen hebben. Ook mag u geen aandoening van het centraal zenuwstelsel hebben (bijvoorbeeld als gevolg van een hoofdletsel).

Vertrouwelijkheid van gegevens
Na het verkrijgen van uw informatie zullen we vertrouwelijk met deze gegevens omgaan. Wij zullen ervoor zorgen dat niet bevoegde buitenstaanders geen inzage hebben in uw gegevens. Uw gegevens worden met een bepaalde code bewaard. Wanneer het onderzoek gepubliceerd wordt, zal informatie over u niet op u terug te herleiden zijn.

Verzekering
Omdat deelname aan het onderzoek geen risico met zich meebrengt voor de deelnemers, heeft de Commissie Medische Ethiek van het LUMC ontheffing van verzekering verleend.

Betekenis van het onderzoek
Omdat het onderzoek zich in een verkennende fase bevindt, kunnen wij u geen individuele uitslag geven van het onderzoek. Wel zullen we u op de hoogte houden van het verloop van

het onderzoek.

Vrijwillige deelname
Deelname aan dit onderzoek geschiedt geheel vrijwillig. Het staat u geheel vrij om wel of niet mee te doen. Ook al hebt u op een bepaald moment schriftelijk toestemming gegeven voor het onderzoek, dan kunt u dat te allen tijde weer intrekken zonder dat dit enige gevolgen heeft.

Als bijlage treft u een antwoordformulier waarop u kunt aangeven of u wel of niet bereid bent deel te nemen aan het onderzoek. Ik wil u verzoeken dit formulier in te vullen en op te sturen in de bijgesloten antwoordenvelop (een postzegel is niet nodig). U kunt ons ook per e-mail laten weten of u wel of niet bereid bent deel te nemen aan het onderzoek (in dat geval dient u het originele ingevulde formulier mee te nemen op de dag van het onderzoek). Indien u bereid bent deel te nemen, verzoeken wij u ook de bijgevoegde vragenlijst in te vullen en op te sturen, zodat wij kunnen bepalen of u geschikt bent om aan dit onderzoek deel te nemen. Zodra uw antwoordformulier bij ons is binnengekomen, zal contact met u worden opgenomen.

Nadere informatie
Indien u nog vragen heeft over het onderzoek, kunt u contact opnemen met ondergetekende. Daarnaast kunt u voor vragen ook een onafhankelijk arts benaderen, te weten dr. J Marinus, afdeling neurologie van het LUMC, telefoonnummer 071 526 4640. Dr. Marinus is niet bij het onderzoek betrokken, maar is wel op de hoogte van de inhoud van dit onderzoek.

Wij danken u bij voorbaat hartelijk voor de eventuele medewerking.

Met vriendelijke groet,

Mw. P.J.M. Bank, MSc., onderzoeker
LUMC, afdeling Neurologie
Telefoon: 071 526 3661

Dhr. L.R.M. Dobbe, BSc., onderzoeker
TUDelft
Telefoon: 06-14204718

E-mail: neuras_onderzoek@lumc.nl

A-2 Informed Consent

Toestemmingsformulier voor deelname aan het wetenschappelijk onderzoek
"NEURAS-V: Invloed van visuele informatie op het motorisch gedrag"

In te vullen door de proefpersoon:

Ik heb de informatiebrief gelezen en ben WEL / NIET* bereid deel te nemen aan bovengenoemd onderzoek. (* Doorhalen wat niet van toepassing is.)

Indien de vorige vraag met 'WEL' beantwoord is, betekent dat het volgende:

- U bent naar tevredenheid geÃŕnformeerd over het onderzoek;
- U heeft voldoende tijd gehad om te beslissen of u meedoet;
- U gaat akkoord met een bewegingsonderzoek in het LUMC;
- U zich realiseert dat u geen onderzoeksuitslag voor uzelf kunt verwachten.

Naam en voorletters: ..... M / V
Telefoon overdag: .....
Telefoon 's avonds: .....
Geboortedatum: .....
EâĂŘmailadres: .....

Handtekening: .....
Datum: .....

In te vullen door de onderzoeker:

Ik verklaar hierbij dat ik deze proefpersoon volledig heb geÃŕnformeerd over het genoemde onderzoek. Als er tijdens het onderzoek informatie bekend wordt die de toestemming van de proefpersoon zou kunnen beÃŕnvloeden, dan breng ik hem/haar daarvan tijdig op de hoogte.

Naam onderzoeker (of diens vertegenwoordiger): .....
Handtekening: .....
Datum: .....

A-3 Experiment Questionnaire

This section presents the questionnaires and its results. The questionnaires consisted of 16 theorems for experiment 1 and 15 theorems for experiment 16. Subjects had to indicate to which degree (0: absolutely no agreement, 10: total agreement) they agreed to the theorem. The results are displayed in Figure A-1 (experiment 1) and Figure A-2 (experiment 2).

A-3-1 Experiment 1

The theorems consisted of the following:

1. I used the full width of the road at all times.
2. I tried to keep the car at the center of the road at all times.
3. I had control over the WA at all times.
4. The experiment varied in difficulty.
5. The narrowing of the road made the task more difficult.
6. The truck that prevented from seeing the road made the task more difficult.
7. The increases in velocity made the task more difficult.
8. Because of the changes in visual feedback, I adapted my motor control to ensure high performance.
9. I was distracted during the experiment.
10. The experiment was boring.
11. I have concentrated well during the entire experiment.
12. The task motivated me enough to perform well.
13. The performance feedback motivated me enough to perform well.
14. During the experiment I suffered from fatigued muscles.
15. During the experiment I lost muscle power.
16. The pauses were long enough to let my muscles recover.

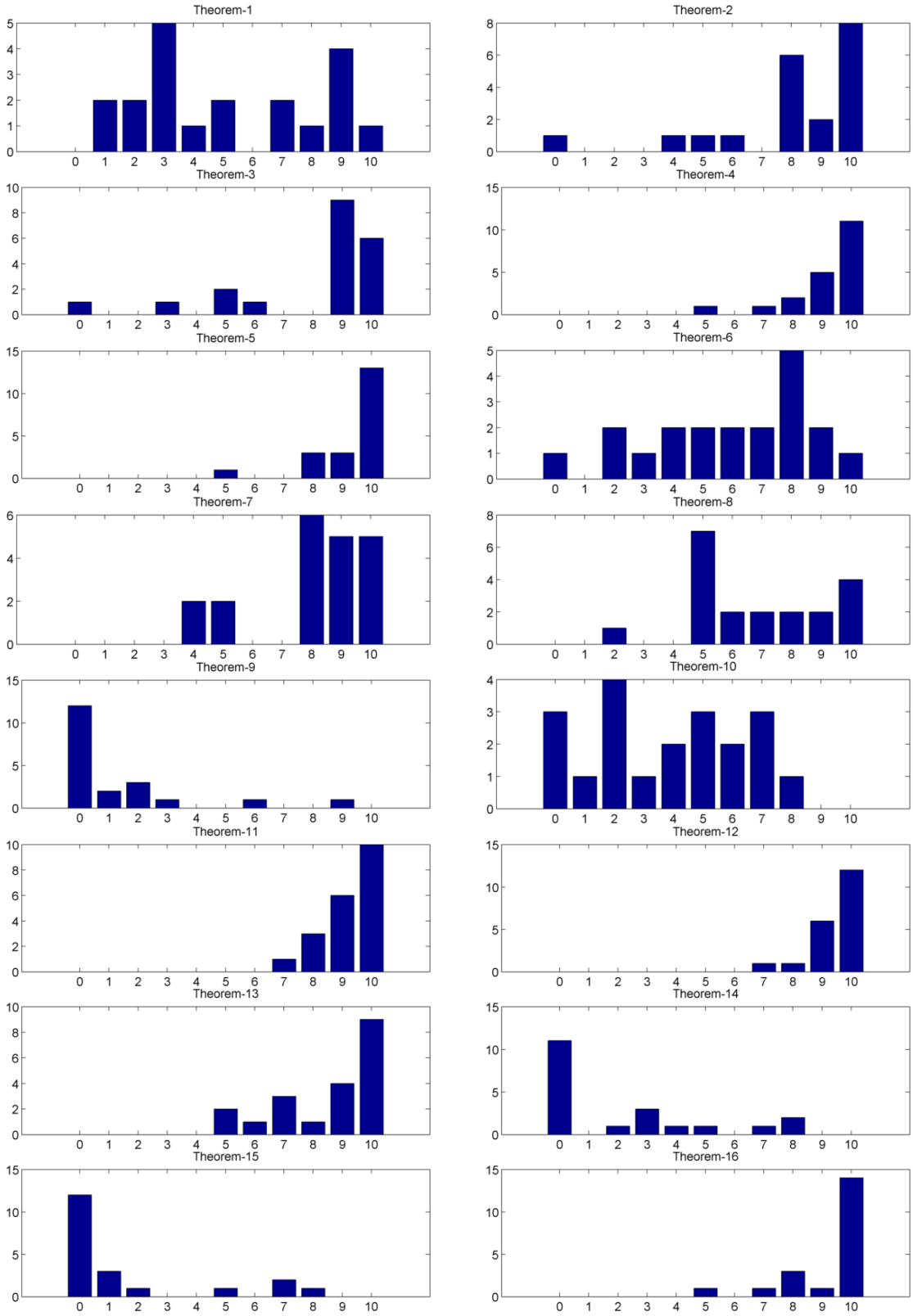

Figure A-1: Questionnaire results for experiment 1 for all healthy (20) subjects. The results are related to the theorems stated in Section A-3-1. Subjects had to indicate to which degree they agreed with a theorem (0 = absolutely no agreement, 10 = total agreement).

A-3-2 Experiment 2

1. I used the full width of the road at all times.
2. I tried to keep the car at the center of the road at all times.
3. I had control over the WA at all times.
4. The experiment was difficult.
5. The presence of the tunnel made the task more difficult.
6. The task varied in difficulty.
7. Because of the changes in visual feedback, I adapted my motor control to ensure high performance.
8. I was distracted during the experiment.
9. The experiment was boring.
10. I have concentrated well during the entire experiment.
11. The task motivated me enough to perform well.
12. The performance feedback motivated me enough to perform well.
13. During the experiment I suffered from fatigued muscles.
14. During the experiment I lost muscle power.
15. The pauses were long enough to let my muscles recover.

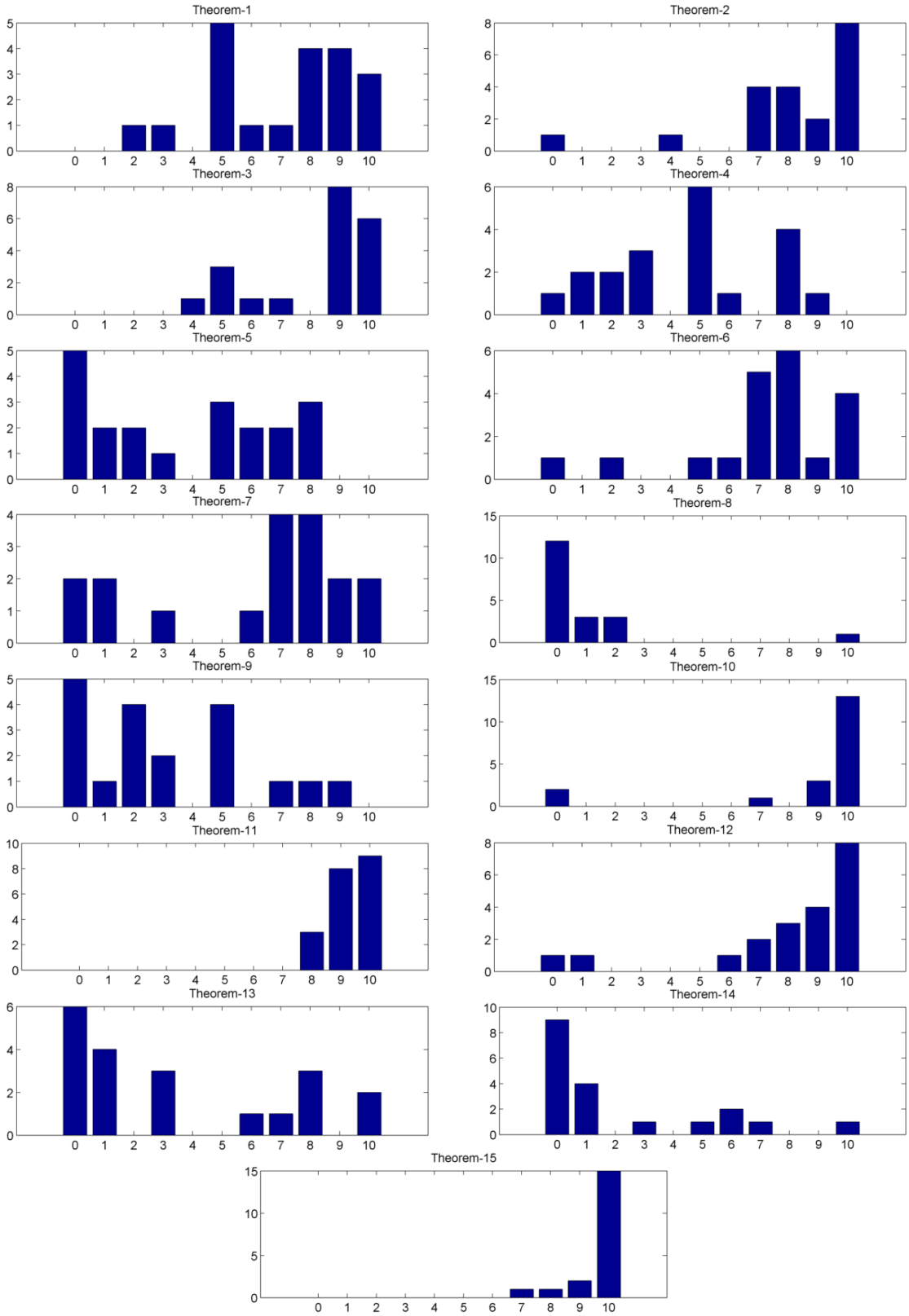

Figure A-2: Questionnaire results for experiment 2 for all healthy (20) subjects. The results are related to the theorems stated in Section A-3-2. Subjects had to indicate to which degree they agreed with a theorem (0 = absolutely no agreement, 10 = total agreement).

A-4 Pain Questionnaire

The pain questionnaire consisted of 4 questions. Subjects could indicate, on a scale of 0 (no pain) to 10 (unbearable pain), how much pain they suffered before, during and after the experiment. Question 4 was scaled as 0: not stressful, to 10: very stressful.

Questions:

1. How much pain did you experience before the experiment?
2. How much pain did you experience right after the experiment?
3. How much pain did you experience on average?
4. How stressful was the execution of the task?

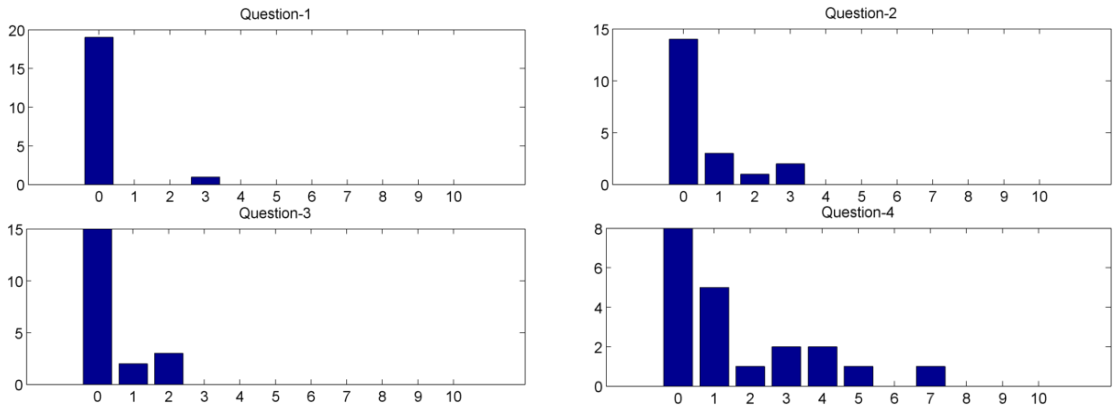

Figure A-3: Pain questionnaire results for all healthy subjects (20). The figures are related to the questions posed in Section A-4. For question 1 to 3 holds: 0 = no pain, 10 = unbearable pain. For question 4 the scale is represented by: 0 = not stressful, 10 = very stressful.

Appendix B

Literature Study

B-1 Literature Study: Visual Information in Motor Control

The purpose of this research is to investigate whether visual sensory input influences task performance during a motor task. Therefore, it is essential to understand the mechanisms of the visual system by means of a literature study. This section provides a summary of a literature survey which has been conducted prior to this master thesis, and highlights the visual conditions found to influence motor task performance.

B-1-1 Visual Feedback to Motor Command

The visual brain processes information through two pathways: 1) the ventral flow, which takes account of object recognition (i.e., properties such as color, texture and shape) and communication with cognitive brain areas, and 2) the faster dorsal flow, which is responsible for motion coding (i.e., properties such as luminance, orientation and size) and communication with the motor areas in the brain (Mishkin et al., 1983; Faillenot et al., 1997; Veerman et al., 2008; Brenner and Smeets, 2003; Milner and Goodale, 1995). The sensory system gives humans the capability to estimate spatial features (e.g., size, shape and position). Recent belief is that the brain acts like a near-optimal Bayesian estimator, in which an estimate of the state is obtained based on the uncertainties of the provided sensory input (Jacobs, 2002). However, if other senses are unavailable (e.g., when the size of an object at a distance needs to be estimated) the visual system remains able to accurately estimate spatial properties. Hence, the visual system continuously estimates **spatial conditions** and it is therefore likely that spatial features of visual feedback play a significant role in the interaction with the environment and the coördination of movements.
Although the visual system provides a very detailed spatial feedback state of the environment, the visual processing time is relatively high (200 ms, (Brenner and Smeets, 2003)). Furthermore, the processing of visual information for corrective movements is much faster (100 ms, (Veerman et al., 2008)). This poses limits to the kind of movements visual information can be used for as sensory feedback and feed-forward information (note: strictly,

visual information is *always* feedback. However, it may be used to plan motor commands in a future state (Krishnan et al., 2012), which may be interpreted as feed-forward information for motor output). In other words: the visual system is bound to **temporal conditions**.

Following prior reasoning, it is fair to divide visual feedback into *spatial* and *temporal* properties. Section B-1-2 will introduce spatial and temporal conditions found to have influence on movement behavior.

B-1-2 Visual Attributes

This subsection discusses the spatial and temporal attributes proven to have influence on movement behavior. The discussed attributes are included in the research protocol, which will be discussed in Section 2-1.

Spatial Attributes

Movement Tolerance The movement tolerance describes the boundaries to which a movement is limited. For instance, driving a car through a narrow street is a movement task with a low movement tolerance, while driving over an empty high way provides a high movement tolerance. While the actual constraints which define the tolerance are strictly physical, they are fed back visually. When movement tolerances decrease, more effort is needed to complete the task, which results in an increased end-point stiffness (Selen et al., 2006b) in pointing tasks as well as an increased arm stiffness in tracking tasks (Selen et al., 2006a) and an overall better performance (i.e., reducing the (pointing or tracking) position error). Although the decrease in movement tolerance influences movement control, it is not known which underlying control mechanisms are influenced. The aim of present study is to identify these mechanisms.

Visual Gain The visual gain is the degree to which a movement magnitude is amplified. A high visual gain is provided by e.g., looking through a magnifying glass or a microscope. When movement errors are amplified in force and position error control tasks, humans perform better (i.e., a higher error reduction). However, the visual gain may also become too high, which results in unstable movement behavior (i.e., previous movements are continuously compensated with movement overshoots in the opposite direction) (Beuter et al., 1995; Vaillancourt et al., 2006; Hong and Newell, 2008). It is likely that an increased visual gain results in a higher limb impedance. However, it is not yet known which neuromuscular mechanisms are responsible for this behavior.

Optical Flow and Velocity The optical flow defines the amount of spatial information available that gives humans the perception of movement velocity and direction. For instance, driving though a tunnel provides a complete view of the velocity and the direction, while driving a car in a countryside environment only provides optical flow information from the ground and possibly also the periphery (e.g., trees, houses). Experiments with optical flow fields (i.e., a field that consists of moving stripes originating from a certain point in a two dimensional field) showed that humans' tracking performance improved when the density and

the velocity of the moving stripes increased (Berntsen et al., 2005). It indicates that if more visual information is available, humans are better able to estimate tracking errors and therefore are capable to improve movement control. It is not known however, which underlying neuromechanical mechanisms contribute to this behavior.

Temporal Attributes

Preview The preview defines the amount of visual information about the movement task that is available on forehand i.e., the amount of information that can be used to anticipate to future events. For instance, driving a car on an empty high way provides a high preview, since the driver is able to look ahead and therefore capable of anticipating to the road. However, when a large car is driving in front of the driver, less information about the future road development is available. The driver therefore has less time to anticipate to the road and most likely will adjust his movement control accordingly.

Discussion

The presented visual attributes each have proven to have influence on movement control. One could argue that the proposed attributes 'movement tolerance', 'velocity' and 'preview' influence movement control behavior due to their physical meaning rather than their visual properties, since these attributes can be translated to a physical quantity. However, the feedback of these attributes is presented visually to the human body. On the contrary, the attributes 'visual gain' and 'optical flow' do describe a visual property.

Appendix C

Methods

C-1 Hardware Delay

Since this research concerns human-machine interaction, it is of importance to expose the hardware delay, which is the delay from mechanical input (i.e., rotation of the WA) to visual output (i.e., the control variable linked to the position of the WA, represented in the virtual environment). Preferably, this delay should be lower than 100 ms, since higher time delays may give the WA a sloppy feel (Miall et al., 1985). Moreover, experimentally imposing a delay of more than 100 ms onto visual feedback in a human manual tracking task immediately causes increased performance errors (Foulkes and Miall, 2000).
The hardware delay of the experimental setup was estimated by using object recognition software of the Computer Vision Toolbox of Matlab. In a simple D-Flow application, the rotation of the WA was linked to the x (lateral) position of a white square in the virtual environment. A position sinusoid, with a frequency of 1, 1.5 or 2 Hz, was applied to the WA. A green squared piece of carton was glued to the WA to track the WA position. Subsequently, the movement of both the WA's piece of carton and the white square on the TV monitor were captured in the same video. With the use of the Computer Vision Toolbox of Matlab and optimization algorithms, the time delay of the white square with respect to the square on the WA could be calculated.
The calculated time delay, for the three different sinusoids, was approximately **135 ms** (1 Hz: 133 ms, 1.5 Hz: 137 ms and 2 Hz: 135 ms). Unfortunately, the time delay could not be decreased, since it was caused by the WA Application Programming Interface (API). The found hardware delay however, was considered in the analysis of the results.

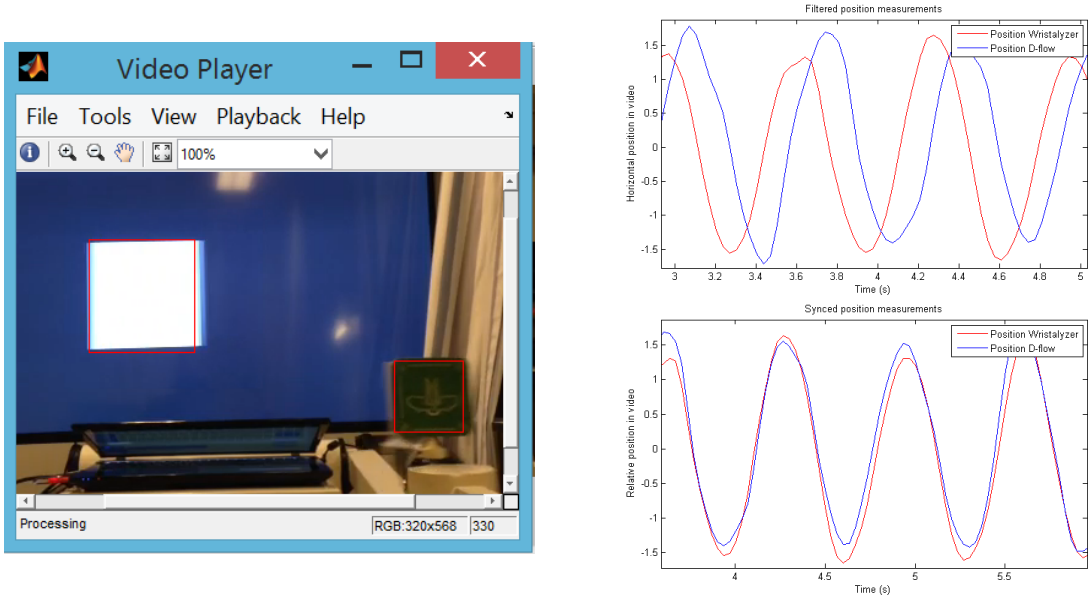

Figure C-1: The white and the green square tracked by the Computer Vision Toolbox (a) and The position responses of the squares (top) and the time shift result which determined the time delay (b)

C-2 Condition Tables

Condition	Velocity [DFU/s]	Preview [DFU]	Movement Tolerance [DFU]
1	4	2	0.25
2	8	2	0.25
3	12	2	0.25
3	12	2	0.25
4	4	2	0.5
5	8	2	0.5
6	12	2	0.5
7	4	2	1.5
8	8	2	1.5
9	12	2	1.5
10	4	10	0.25
11	8	10	0.25
12	12	10	0.25
13	4	10	0.5
14	8	10	0.5
15	12	10	0.5
16	4	10	1.5
17	8	10	1.5
18	12	10	1.5
19	4	50	0.25
20	8	50	0.25
21	12	50	0.25
21	12	50	0.25
22	4	50	0.5
23	8	50	0.5
24	12	50	0.5
25	4	50	1.5
25	4	50	1.5
25	4	50	1.5
26	8	50	1.5
27	12	50	1.5
HS	12	50	0.25
ES	4	50	1.5

Table C-1: The condition table for experiment 1 sorted by visual attribute

Condition	Visual Gain	Road Width [DFU]	Car Scale [DFU]	Tunnel [1=yes, 0=no]
1	1	0.6	1	0
2	1	0.6	1	1
3	2	1.2	2	0
4	2	1.2	2	1
5	4	2.4	4	0
6	4	2.4	4	1

Table C-2: The condition table for experiment 2 sorted by visual attribute

C-3 Perturbation Signal Time Length

Three signals (2s, 4s and 8s) were assessed to determine the appropriate perturbation signal time length for the experiments. For each of these signals a TV analysis was done for time windows of the perturbation signal length and for each 1 second shorter, to a minimum of 1 second (i.e., for the perturbation signal of 8 seconds, 8 analyses were done: 8s, 7s,..., 1s etc.). The goal of this analysis was to determine the appropriate signal length for the study design, and to determine whether it is possible to analyze the data with time windows which are shorter than the perturbation signal length. The obtained results were validated with the VAF of the simulated position response of the identified ARMAX models. The obtained data is based on one test subject for a measurement of two conditions (i.e., hard condition to easy condition) and a transition in between. The transition phase is depicted by black circles (from 40 - 50 s). It was expected that the VAF would drop at the moment the test subject changed motor behavior to adapt to the new condition.

Results From the figures it is clear that short time windows are capable of a correct estimation of the model. It is striking that the VAF values remain high (>90%) using a signal length of 8 seconds and time windows of only 1 or 2 seconds (Figure C-2a). Furthermore, on average, the VAF values of short time windows are higher than those of the longer time windows. As expected the VAFs drop at the moment the test subject adapts its control strategy. This is more apparent at higher time windows than for low time windows (see Figure C-2c). This could indicate that motor adaptations appeared at a frequency of 1 Hz.

Conclusions The pilot test analysis showed that time window analyses with time windows shorter than the perturbation signal length yield high VAF model responses. Therefore, one could conclude that the perturbation time length is not an important aspect. However, the time length also defines the frequency resolution for the spectral analysis. Although ARMAX modeling techniques are used for the identification, a spectral analysis is a simple and fast validation method for the identified ARMAX model. Therefore, signals of 1 and 2 seconds are too short, since (considering averaging over 4 frequency bands) this results in a frequency resolution of approximately 4 and 2 Hz, which is too low to identify sufficient details in a frequency response. Therefore, a perturbation signal length of 4 seconds is chosen (frequency resolution = 1 Hz).

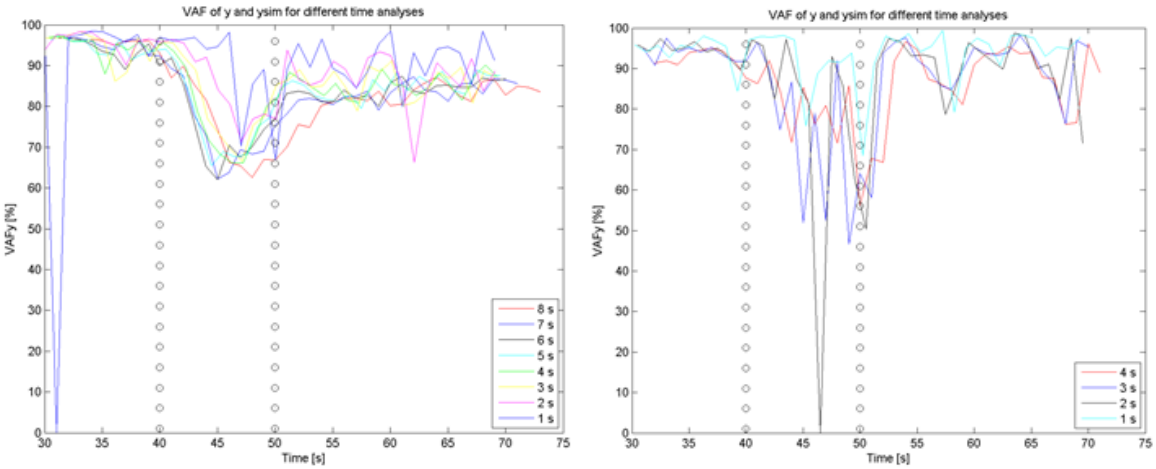

(a) The analysis for a time window of 8 seconds **(b)** The analysis for a time window of 4 seconds

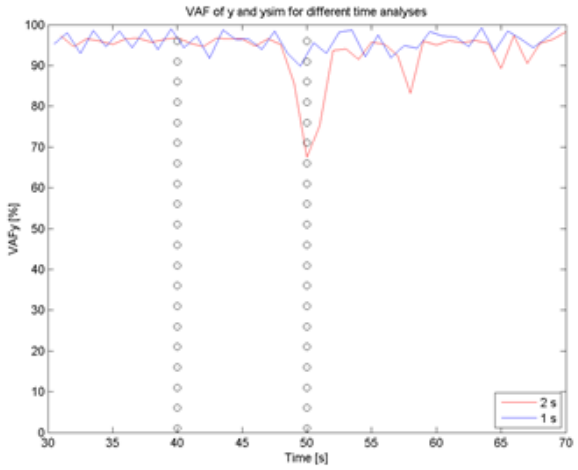

(c) The analysis for a time window of 2 seconds

Figure C-2: The perturbation signal time length analysis for 8s (a), 4s (b) and 2s (c) for two conditions and a transition phase. The graphs describe the found VAFs for a TV analysis of the perturbation signal length and each second shorter (i.e., figure (a) shows the responses for 8, 7, 5,.., 1 second). Lines left from the first vertical black circle line are the found VAFs for the easy condition, the transition phase is the area between the two vertical black circle lines and the lines right from the right vertical circle line describe the found VAFs for the hard condition.

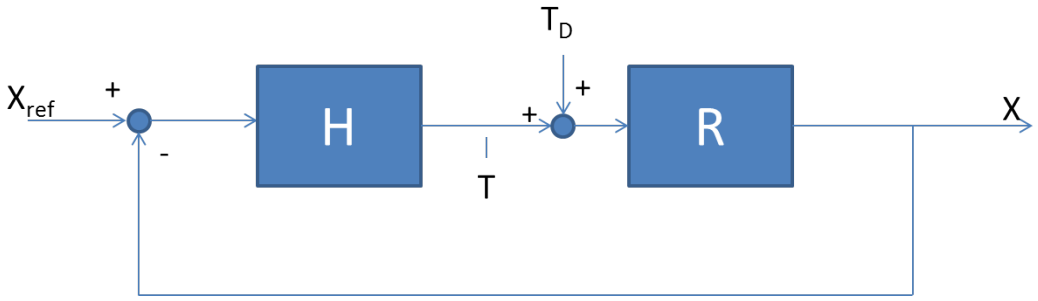

Figure C-3: The (simplified) control scheme, presenting the interaction of the human (H) with the robot (R) while minimizing the position of the car (X) with respect to the position of the road (X_{ref}) and being subjected to external force perturbations (T_D).

C-4 Closed Loop Estimator

The entities in Figure C-3 represent the input signals, the measured signals and the interacting dynamic systems described by the human and the robot:

- Input signals:
  T_D. The perturbation signal (i.e., the disturbance torque) [Nm].
  X_{ref}. The road position [rad].
- Measured signals:
  X. The measured car position [rad].
  T. The measured torque exerted on the WA, measured by the force sensor [Nm].
- The dynamic systems:
  H. The lumped human control dynamics at the wrist, described by the joint admittance [rad/Nm] (i.e., the joint displacement as a result of the input torque).
  R. The Robot dynamics.

The objective is to identify the contribution of the human (H). First the measured signals $X(k)$ and $T(k)$ are defined by the open loop responses of $T_D(k)$ to $T(k)$ and $T_D(k)$ to $X(k)$:

$$T(k) = \frac{H}{1+HR}X_{ref}(k) + \frac{HR}{1+HR}T_D(k) \tag{C-1}$$

$$X(k) = \frac{HR}{1+HR}X_{ref}(k) + \frac{R}{1+HR}T_D(k) \tag{C-2}$$

Influence from X_{ref} (0.08 - 0.25 Hz) was assumed to be marginal, since the measured output signal X was high pass filtered ($>$ 2 Hz) to eliminate low frequent responses. Therefore (C-2) and (C-1) result in:

$$\frac{T(k)}{T_D(k)} = \frac{HR}{1+HR} = H_{T_DT} \tag{C-3}$$

$$\frac{X(k)}{T_D(k)} = \frac{R}{1 + HR} = H_{T_D X} \tag{C-4}$$

H can now be estimated by:

$$\frac{H_{T_D T}}{H_{T_D X}} = H \tag{C-5}$$

C-5 ARMAX Model Order

Introduction The goal of this analysis is to assess different ARMAX model structures. One test subject executed a tracking task in the course of two successive conditions (from hard to easy) by controlling the WA. Subsequently, a TV analysis was done on the data. The appropriate order was chosen from an ARMAX order analysis based on the model VAFs, in which the first half of the time data was used to build the model, and the second half was used to validate the model and calculate the VAF. The two conditions are considered to be the most difficult and the easiest.

The ARMAX model needs to comprise all neural and mechanical wrist dynamics. To prevent over and under fitting of the ARMAX model the correct order needs to be determined before a proper analysis can be performed. The ARMAX model orders are determined by varying the model orders over n = 6, 8, 10, 12 and 14. A time window of 4 seconds and 2 seconds respectively was slided over the measurements in steps of 1 second (see Figure 2-8). The measurement consisted of 30 seconds of hard condition, 10 seconds of transition and 30 seconds easy condition. By analyzing the VAFs of different orders, the optimal order can be obtained. The model orders that characterize an ARMAX model were kept equal with respect to each other, while they were varied (n = [6, 8, 10, 12, 14], na = nb = nc = n and nk = 0). Figure C-4a and Figure C-4b show the obtained VAFs for t_{window} = 4 s and t_{window} = 2 s, respectively. The results for each order are depicted as lines, whereas the transition area is depicted by two vertical lines (black circles) at t = 30 s and t = 40 s.

Observations The simulated responses for orders n = 10, 12 and 14 (not shown in figures) were unstable, which indicates over-fitting of the model structure. The simulated responses for t_{window} = 2 s and n = 10 also showed unstable behavior. The results for orders n = 6 and n = 8 are largely equal, which indicates that most dynamics of the system are included in a model with order n = 6 and n = 8 order model. As expected a 'dip' shows in the transition area (between 30 s and 40 s). This dip is more apparent for a time window of t = 4 s, probably because the change in control behavior was shorter than 4 s which means that multiple time windows included the control change,

Conclusions Based on the results the best choice is order n = 8. Although results for n = 6 were comparable, they were only based on one test subject. To prevent possible under-fitting for other test subjects, it is therefore better to choose a somewhat higher model order.

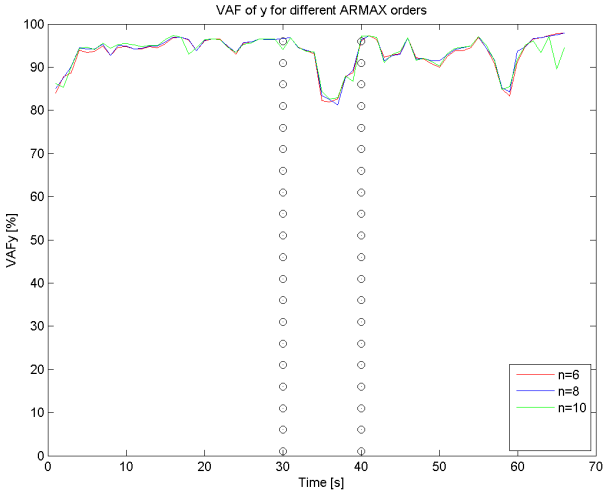

(a)

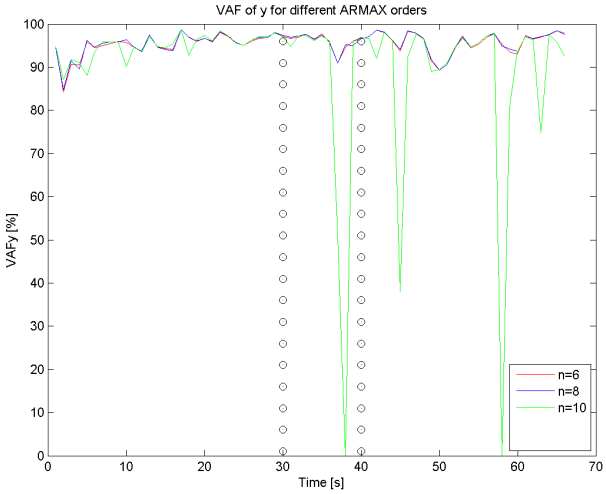

(b)

Figure C-4: The VAFs for ARMAX models with order 8, 9, 10 (12, 14 are not shown), for a time window of 4 s (a) and 2 s (b). Simulated responses for orders of 12 and 14 were unstable and therefore not shown. The lines show the VAFs for the hard condition (left from the left black lines), the transition phase (in between the black circle lines) and the easy condition (right from the right black circle line).

C-6 Parameter Model Choice

Three different neuromuscular models, a 'reflexive model' (Figure C-5a), a 'visual model' (Figure C-5b) and a 'visual-reflexive model' (Figure C-5c), were assessed on the data of experiment 1 of 5 subjects. Contributions of force feedback (Golgi tendon organs) and position feedback (muscle spindles) were not taken into account, since earlier tests returned extremely high SEM values, indicating low contributions of these parameters to the model fit.

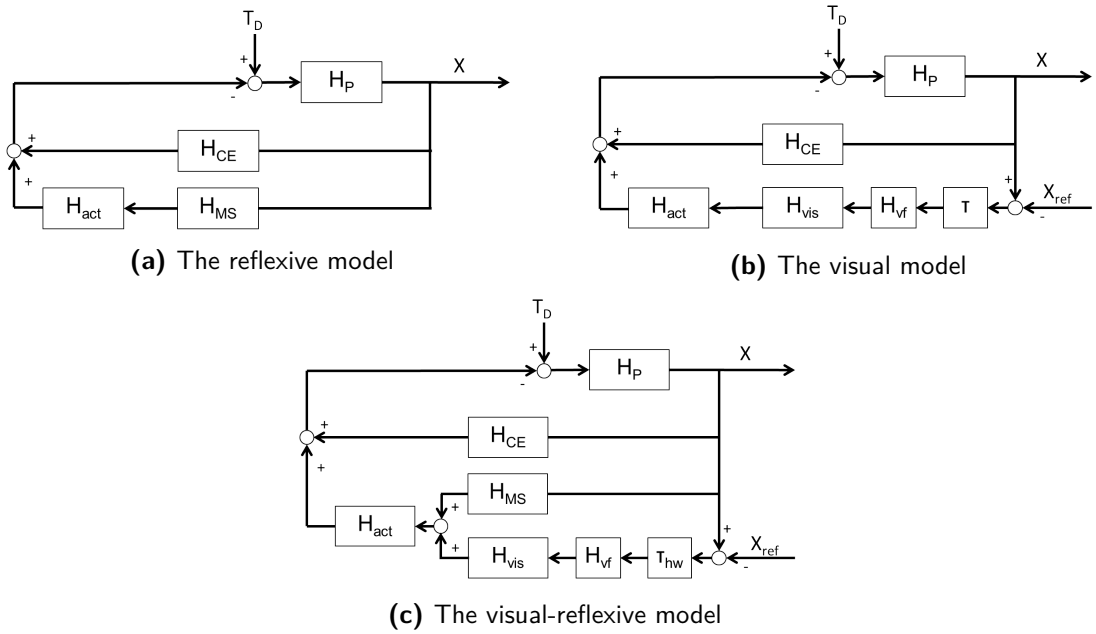

(a) The reflexive model

(b) The visual model

(c) The visual-reflexive model

Figure C-5: The neuromuscular models that are assessed with the test data of five subjects to choose the appropriate model.

The models were assessed by two criteria:

1. The model fit error of the total time data parameter estimation (i.e., a model fit over the total measurement data per condition (= 20 s), for all conditions of experiment 1, for 5 subjects.

2. SEM values of all obtained neuromuscular parameters from the three models.

The model that yielded the lowest model fit errors and lowest SEM values for the parameters was chosen. Figure C-6a shows the mean fit error (see Equation (2-8)) per subject, averaged over all conditions for the total time span of the conditions. Figure C-6b shows the mean fit error per subject, averaged over all conditions and over all time windows for the TV analysis. Figure C-6b depicts the average SEM values of the parameters of interest (k_v, τ_d, k_{vis} and τ_{dvis}).

Observations Figure C-6a shows that the visual-reflexive model holds a somewhat better model fit than the reflexive model. However, it is not desirable to have an over-parameterized

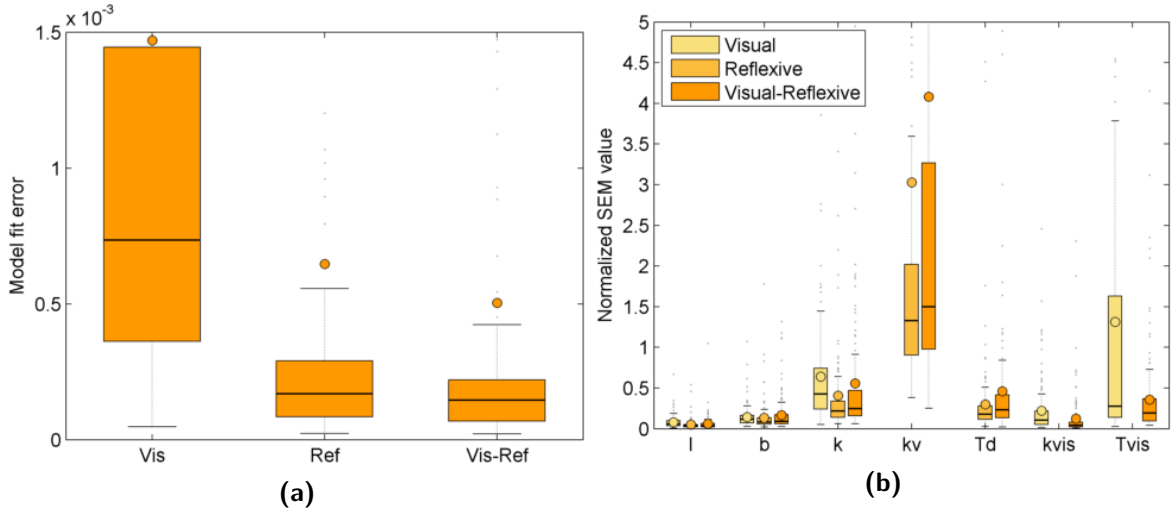

Figure C-6: (a): Boxplot of the obtained model fit error of the Visual model (Vis), the Reflexive model (Ref) and the Visual-Reflexive model (Vis-Ref) for all conditions of experiment 1, for 5 subjects. (b): A boxplot of the corresponding normalized (to parameter value) SEM values of the obtained neuromuscular parameters. Boxplots illustrate the median (-), the 25th (Q1) and 75th (Q3) percentiles and the means (○).

model (i.e., a model with a low model fit error, defined by too many parameters). To identify an over-parameterized model the parameter SEM value can be used. Figure C-6b shows the SEM values for the parameters of interest. The visual-reflexive model contains two extra parameters from which three return low SEM values and one, which is k_v, returns somewhat higher SEM values to those of the reflexive model. However, the combination of the visual and reflexive pathways results in lower SEM values for k_{vis} and τ_{vis} in the visual-reflexive model than in the visual model, which indicates that this parameter fits better in this model structure.

Model choice Based on the found model fit errors, the visual model can directly be excluded. Errors for the visual-reflexive model are somewhat lower than for the reflexive model, but return relatively higher SEM values for k_v, which could indicate signs of over-parameterization. However, the combination of the reflexive and the visual pathways decreases SEM values for the visual parameters (and thus a higher reliable estimation of those parameters). It could be that an unknown contributor is caught by k_v and therefore does not interfere with contributions of k_{vis}. This also explains the improved parameter fit. Moreover, from the research topic point-of-view, it is desirable to study influences of long-latency reflexes (i.e., the visual pathway). Therefore, the visual-reflexive model was chosen, with the cost that contributions of k_v and τ_d were relatively less reliable.

C-7 Parameter Model

Figure C-7 illustrates the model to which the obtained measurement data were fitted. This section describes the implementation and optimization of the model.

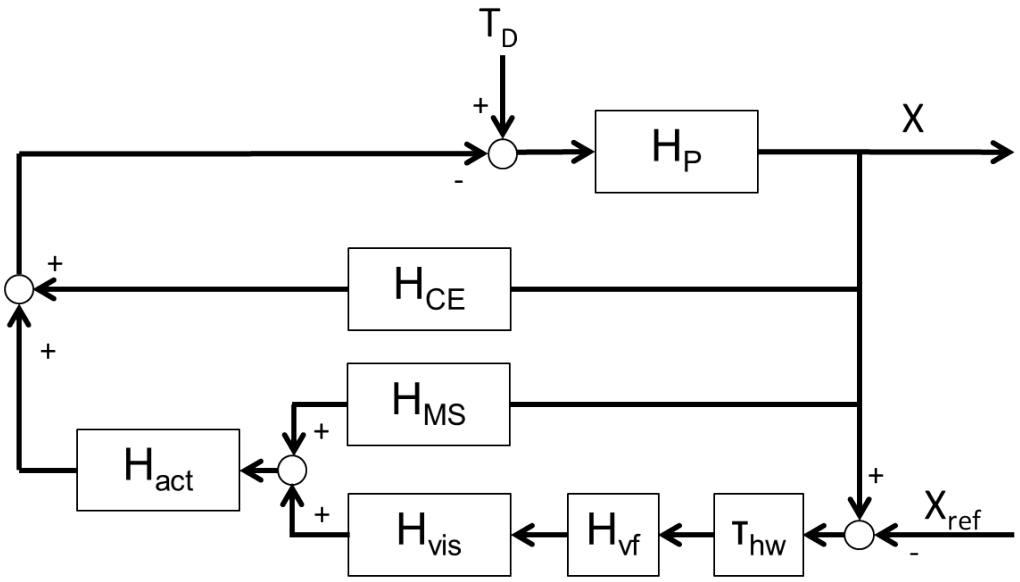

Figure C-7: The parametric model for H

The input signals are represented by the force perturbation (T_D) and the input reference position (X_{ref}) and the output signal is the measured WA rotation (X). The blocks in the parameter scheme are represented by the following parameters:

$$H_p = \frac{1}{I_{wr}s^2} \tag{C-6}$$

The passive wrist dynamics, described by the wrist inertia.

$$H_{CE} = bs + k \tag{C-7}$$

The contractile elements (active dynamics) of the wrist joint, described by the muscle stiffness and damping.

$$H_{MS} = k_v s e^{-T\tau_{ms}s} \tag{C-8}$$

Reflexive muscle spindle velocity feedback, described by a gain velocity k_v and a neural time delay τ_d.

$$H_{vis} = k_{vis} e^{-\tau_{vis}s} \tag{C-9}$$

Visual feedback, described by a position gain k_{vis} and a neural time delay τ_{vis}.

$$H_{vf} = \frac{1}{1 + 0.1s} \tag{C-10}$$

The visual filter of high frequent perturbations in the visual feedback

$$\tau_{hw} = e^{-0.135s} \tag{C-11}$$

The visualization delay of the software (135 ms).

$$H_{act} = \frac{\omega_0^2}{s^2 + 2\beta\omega s + \omega_0^2}, \omega_0 = 2\pi f_0 \tag{C-12}$$

The activation dynamics.

The parameter model was fitted to the frequency response of the ARMAX model by means of non-linear least squares optimization in the frequency domain. The error between both models was defined as the squared logarithmic difference between the frequency responses of both models. Relatively higher weight was given to the lower frequencies and to frequencies with a high coherence:

$$E(f) = |log(\frac{H_A(f)}{H_{par}(f)})| \ \cdot \ \frac{1}{f} \ \cdot \ \gamma^2(f) \tag{C-13}$$

Equation (C-13) was minimized based on the parameter vector:

$$P = [I_{wr} \ b \ k \ k_v \ \tau_d \ k_{vis} \ \tau_{vis}]^T \tag{C-14}$$

Prior to optimization, P was normalized to the start vector P_0. Consequently, the obtained SEM values were also normalized. Optimization start values (P_0), as well as lower (P_{lo}) and upper (P_{hi}) boundary values are presented in Table C-3.

Table C-3: Parameter optimization settings, consisting of the start values (P_0), as wel as lower (P_{lo}) and upper (P_{hi}) boundary values.

	I_{wr} $10^{-3}[kg/m^2]$	b $[Nms/rad]$	k $[Nm/rad]$	k_v $[Nms/rad]$	τ_d $[ms]$	k_{vis} $[Nm/rad]$	τ_{vis} $[ms]$
P_0	50	0.05	1	0.01	30	2	150
P_{hi}	100	1	50	10	200	10	350
P_{lo}	10	0.001	0.01	-10	15	0.01	80

Bibliography

Bays, P. M. and Wolpert, D. M. Computational principles of sensorimotor control that minimize uncertainty and variability. *The Journal of Physiology*, 578(2):387–396, 2007. ISSN 1469-7793. doi: 10.1113/jphysiol.2006.120121.

Berntsen, M., Mulder, M., and Van Paassen, M. Modelling human visual perception and control of the direction of self-motion. In *Proceedings of the AIAA Modeling and Simulation Technologies Conference & Exhibit, San Francisco, CA*, 2005.

Beuter, A., Haverkamp, H., Glass, L., and Carrière, L. Effect of manipulating visual feedback parameters on eye and finger movements. *International Journal of Neuroscience*, 83(3-4): 281–294, 1995.

Brenner, E. and Smeets, J. B. Perceptual requirements for fast manual responses. *Experimental brain research*, 153(2):246–252, 2003.

Brink, E., Jankowska, E., McCrea, D., and Skoog, B. Inhibitory interactions between interneurones in reflex pathways from group ia and group ib afferents in the cat. *The Journal of physiology*, 343(1):361–373, 1983.

de Vlugt, E., Schouten, A. C., and van der Helm, F. C. T. Adaptation of reflexive feedback during arm posture to different environments. *Biological Cybernetics*, 87(1):10–26, 2002.

Dobbe, L. The contribution of the visual system to motor control, *Master thesis*, 2014.

Faillenot, I., Toni, I., Decety, J., Grégoire, M.-C., and Jeannerod, M. Visual pathways for object-oriented action and object recognition: functional anatomy with pet. *Cerebral Cortex*, 7(1):77–85, 1997.

Foulkes, A. J. M. and Miall, R. C. Adaptation to visual feedback delays in a human manual tracking task. *Experimental Brain Research*, 131(1):101–110, 2000.

Hong, S. L. and Newell, K. M. Visual information gain and the regulation of constant force levels. *Experimental Brain Research*, 189(1):61–69, 2008.

Ierusalimschy, R., Celes, W., and de Figueiredo, L., 1998. URL www.lua.org.

Jacobs, R. A. What determines visual cue reliability? *Trends in cognitive sciences*, 6(8): 345–350, 2002.

Jankowska, E. and McCrea, D. Shared reflex pathways from ib tendon organ afferents and ia muscle spindle afferents in the cat. *The Journal of physiology*, 338(1):99–111, 1983.

Johnston, I. R., White, G. R., and Cumming, R. W. The role of optical expansion patterns in locomotor control. *The American journal of psychology*, pages 311–324, 1973.

King, M. The interpretation of scores from the eortc quality of life questionnaire qlq-c30. *Quality of Life Research*, 5(6):555–567, 1996. ISSN 0962-9343. doi: 10.1007/BF00439229.

Krishnan, V., Latash, M. L., and Aruin, A. S. Early and late components of feed-forward postural adjustments to predictable perturbations. *Clinical Neurophysiology*, 123(5):1016–1026, 2012.

Loram, I. D., van de Kamp, C., Gollee, H., and Gawthrop, P. J. Identification of intermittent control in man and machine. *Journal of The Royal Society Interface*, 9(74):2070–2084, 2012. doi: 10.1098/rsif.2012.0142.

Meskers, C. G., Schouten, A. C., de Groot, J. H., de Vlugt, E., van Hilten, B. J., van der Helm, F. C., and Arendzen, H. J. Muscle weakness and lack of reflex gain adaptation predominate during post-stroke posture control of the wrist. *Journal of neuroengineering and rehabilitation*, 6:29, 2009.

Miall, R. C., Weir, D. J., Wolpert, D. M., and Stein, J. F. Is the cerebellum a smith predictor? *Journal of Motor Behavior*, 25(3):203–216, 1993. doi: 10.1080/00222895.1993.9942050. PMID: 12581990.

Miall, R. and Jackson, J. Adaptation to visual feedback delays in manual tracking: evidence against the smith predictor model of human visually guided action. *Experimental Brain Research*, 172(1):77–84, 2006.

Miall, R., Weir, D., and Stein, J. Visuomotor tracking with delayed visual feedback. *Neuroscience*, 16(3):511–520, 1985.

Milner, A. D. and Goodale, M. A. *The visual brain in action*, volume 27. England, 1995.

Mishkin, M., Ungerleider, L. G., and Macko, K. A. Object vision and spatial vision: two cortical pathways. *Trends in Neurosciences*, 6(0):414 – 417, 1983. ISSN 0166-2236. doi: http://dx.doi.org/10.1016/0166-2236(83)90190-X.

Mugge, W., Abbink, D., and Van der Helm, F. C. T. Reduced power method: how to evoke low-bandwidth behaviour while estimating full-bandwidth dynamics. In *Rehabilitation Robotics, 2007. ICORR 2007. IEEE 10th International Conference on*, pages 575–581, June 2007. doi: 10.1109/ICORR.2007.4428483.

Mugge, W., Abbink, D. A., Schouten, A. C., Dewald, J. P. A., and Van Der Helm, F. C. T. A rigorous model of reflex function indicates that position and force feedback are flexibly tuned to position and force tasks. *Experimental Brain Research*, 200(3-4):325–340, 2010.

Oldfield, R. C. The assessment and analysis of handedness: the edinburgh inventory. *Neuropsychologia*, 9(1):97–113, 1971.

Sainburg, R., Ghez, C., and Kalakanis, D. Intersegmental dynamics are controlled by sequential anticipatory, error correction, and postural mechanisms. *Journal of Neurophysiology*, 81(3):1045–1056, 1999.

Schmidt, R. A. *Motor learning and performance: a situation-based learning approach*. Human Kinetics, 2008.

Schouten, A. C., Mugge, W., and van der Helm, F. C. Nmclab, a model to assess the contributions of muscle visco-elasticity and afferent feedback to joint dynamics. *Journal of biomechanics*, 41(8):1659–1667, 2008.

Seidler, R., Noll, D., and Thiers, G. Feedforward and feedback processes in motor control. *Neuroimage*, 22(4):1775–1783, 2004.

Selen, L. P. J., van Dieën, J. H., and Beek, P. J. Impedance modulation and feedback corrections in tracking targets of variable size and frequency. *Journal of Neurophysiology*, 2006a.

Selen, L., Beek, P., and van Dieën, J. Impedance is modulated to meet accuracy demands during goal-directed arm movements. *Experimental Brain Research*, 172(1):129–138, 2006b. ISSN 0014-4819. doi: 10.1007/s00221-005-0320-7.

Snedecor, G. and Cochran, W. *Statistical Methods*. 1980.

Steen, J., Damveld, H. J., Happee, R., van Paassen, M. M., and Mulder, M. A review of visual driver models for system identification purposes. In *Systems, Man, and Cybernetics (SMC), 2011 IEEE International Conference on*, pages 2093–2100. IEEE, 2011.

Vaillancourt, D. E., Haibach, P. S., and Newell, K. M. Visual angle is the critical variable mediating gain-related effects in manual control. *Experimental brain research*, 173(4):742–750, 2006.

van der Helm, F. C. T., Schouten, A. C., de Vlugt, E., and Brouwn, G. G. Identification of intrinsic and reflexive components of human arm dynamics during postural control. *Journal of Neuroscience Methods*, 119(1):1–14, 2002.

Van Der Kooij, H. and De Vlugt, E. Postural responses evoked by platform pertubations are dominated by continuous feedback. *Journal of neurophysiology*, 98(2):730–743, 2007.

Veerman, M., Brenner, E., and Smeets, J. The latency for correcting a movement depends on the visual attribute that defines the target. *Experimental Brain Research*, 187(2):219–228, 2008. ISSN 0014-4819. doi: 10.1007/s00221-008-1296-x.

Winters, J. M. and Stark, L. Analysis of fundamental human movement patterns through the use of in-depth antagonistic muscle models. *Biomedical Engineering, IEEE Transactions on*, (10):826–839, 1985.

Wolpert, D. M. and Ghahramani, Z. Computational principles of movement neuroscience. *nature neuroscience*, 3:1212–1217, 2000.